Title
CAR directs T cell adaptation to bile acids in the small intestine

Journal
Nature, 593(7857)

ISSN
0028-0836

Authors
Chen, Mei Lan
Huang, Xiangsheng
Wang, Hongtao
et al.

Publication Date
2021-05-06

DOI
10.1038/s41586-021-03421-6

Peer reviewed

HHS Public Access

Author manuscript

Nature. Author manuscript; available in PMC 2022 February 22.

Published in final edited form as:

Nature. 2021 May ; 593(7857): 147–151. doi:10.1038/s41586-021-03421-6.

CAR directs T cell adaptation to bile acids in the small intestine

Mei Lan Chen[1,2,14], **Xiangsheng Huang**[3,14], **Hongtao Wang**[3], **Courtney Hegner**[1,2], **Yujin Liu**[1], **Jinsai Shang**[4,12], **Amber Eliason**[1], **Huitian Diao**[1,2], **HaJeung Park**[5], **Blake Frey**[6], **Guohui Wang**[3], **Sarah A. Mosure**[1,2,4,7], **Laura A. Solt**[1,2,7], **Douglas J. Kojetin**[2,4,7], **Alex Rodriguez-Palacios**[8,9], **Deborah A. Schady**[10], **Casey T. Weaver**[6], **Matthew E. Pipkin**[1,2], **David D. Moore**[11,13,✉], **Mark S. Sundrud**[1,2,✉]

[1]Department of Immunology and Microbiology, The Scripps Research Institute, Jupiter, FL, USA.

[2]The Skaggs Graduate School of Chemical and Biological Sciences, The Scripps Research Institute, Jupiter, FL, USA.

[3]Section of Gastroenterology, Hepatology, and Nutrition, Department of Pediatrics, Baylor College of Medicine and Texas Children's Hospital, Houston, TX, USA.

[4]Department of Integrative Structural and Computational Biology, The Scripps Research Institute, Jupiter, FL, USA.

[5]X-ray Crystallography Core Facility, The Scripps Research Institute, Jupiter, FL, USA.

[6]Department of Pathology, University of Alabama at Birmingham, Birmingham, AL, USA.

[7]Department of Molecular Medicine, The Scripps Research Institute, Jupiter, FL, USA.

[8]Division of Gastroenterology and Liver Disease, School of Medicine, Case Western Reserve University, Cleveland, OH, USA.

[9]University Hospitals Research and Education Institute, University Hospitals Cleveland Medical Center, Cleveland, OH, USA.

✉**Correspondence and requests for materials** should be addressed to D.D.M. daviddmoore@berkeley.edu or M.S.S. msundrud@scripps.edu.

Author contributions Study design: M.L.C., X.H., H.W., J.S., H.P., B.F., L.A.S., D.J.K., A.R.-P., D.A.S., C.T.W., M.E.P., D.D.M. and M.S.S. Data generation: M.L.C., X.H., H.W., C.H., Y.L., J.S., A.E. and S.A.M. Bioinformatics: M.L.C., H.D., G.W., A.R.-P. and M.E.P. Manuscript: M.L.C., X.H., C.H., A.E., D.J.K., A.R.-P., C.T.W., M.E.P., D.D.M. and M.S.S. Principal investigators: L.A.S., D.J.K., A.R.-P., D.A.S., C.T.W., M.E.P., D.D.M. and M.S.S.

Online content

Any methods, additional references, Nature Research reporting summaries, source data, extended data, supplementary information, acknowledgements, peer review information; details of author contributions and competing interests; and statements of data and code availability are available at https://doi.org/10.1038/s41586-021-03421-6.

Reporting summary

Further information on research design is available in the Nature Research Reporting Summary linked to this paper.

Competing interests M.S.S. is a consultant to Sigilon Therapeutics and Sage Therapeutics.

Additional information

Supplementary information The online version contains supplementary material available at https://doi.org/10.1038/s41586-021-03421-6.

Peer review information *Nature* thanks Richard Blumberg and the other, anonymous, reviewer(s) for their contribution to the peer review of this work.

[10]Department of Pathology and Immunology, Baylor College of Medicine and Texas Children's Hospital, Houston, TX, USA.

[11]Department of Molecular and Cellular Biology, Baylor College of Medicine, Houston, TX, USA.

[12]Present address: Bioland Laboratory, Guangzhou Regenerative Medicine and Health Guangdong Laboratory, Guangzhou, China.

[13]Present address: Department of Nutritional Sciences and Toxicology, University of California Berkeley, Berkeley, CA, USA.

[14]These authors contributed equally: Mei Lan Chen, Xiangsheng Huang.

Abstract

Bile acids are lipid-emulsifying metabolites synthesized in hepatocytes and maintained in vivo through enterohepatic circulation between the liver and small intestine[1]. As detergents, bile acids can cause toxicity and inflammation in enterohepatic tissues[2]. Nuclear receptors maintain bile acid homeostasis in hepatocytes and enterocytes[3], but it is unclear how mucosal immune cells tolerate high concentrations of bile acids in the small intestine lamina propria (siLP). $CD4^+$ T effector (T_{eff}) cells upregulate expression of the xenobiotic transporter MDR1 (encoded by *Abcb1a*) in the siLP to prevent bile acid toxicity and suppress Crohn's disease-like small bowel inflammation[4]. Here we identify the nuclear xenobiotic receptor CAR (encoded by *Nr1i3*) as a regulator of MDR1 expression in T cells that can safeguard against bile acid toxicity and inflammation in the mouse small intestine. Activation of CAR induced large-scale transcriptional reprogramming in T_{eff} cells that infiltrated the siLP, but not the colon. CAR induced the expression of not only detoxifying enzymes and transporters in siLP T_{eff} cells, as in hepatocytes, but also the key anti-inflammatory cytokine IL-10. Accordingly, CAR deficiency in T cells exacerbated bile acid-driven ileitis in T cell-reconstituted *Rag1*$^{-/-}$ or *Rag2*$^{-/-}$ mice, whereas pharmacological activation of CAR suppressed it. These data suggest that CAR acts locally in T cells that infiltrate the small intestine to detoxify bile acids and resolve inflammation. Activation of this program offers an unexpected strategy to treat small bowel Crohn's disease and defines lymphocyte sub-specialization in the small intestine.

To identify the transcriptional mechanisms that underlie local upregulation of MDR1 in siLP T_{eff} cells[4], we considered the ligand-regulated nuclear receptors—environmental-sensing transcription factors that control diverse gene expression programs involved in immunity, inflammation, metabolism and gastrointestinal physiology[5]. To assess the individual contributions of all 49 mouse nuclear receptors to MDR1 expression in mucosal T_{eff} cells, we performed a pooled in vivo RNA interference (RNAi) screen[6]. Activated naive $CD4^+$ T cells transduced separately with 258 retroviruses expressing shRNAmirs (short hairpin RNAs embedded within human microRNA (miR)-30 sequences) against 70 genes (Supplementary Table 1) were pooled, sorted by fluorescence-activated cell sorting (FACS) for retroviral reporter expression, and transferred into syngeneic (FVB/N) *Rag1*$^{-/-}$ mice. Six weeks later, transduced T_{eff} cells were recovered from the spleen or siLP, and $MDR1^{hi}$ or $MDR1^{lo}$ subsets were separated on the basis of ex vivo efflux of the fluorescent MDR1 transport substrate rhodamine 123 (Rh123)[7]. Abundances of shRNAmirs were quantified by DNA sequencing (DNA-seq; Fig. 1a).

Multiple shRNAmirs against *Nr1i3* (encoding CAR) and *Abcb1a* (encoding MDR1 itself) were enriched in MDR1^{lo} versus MDR1^{hi} T_{eff} cells from both spleen and siLP (Fig. 1b, Extended Data Fig. 1a, b). As CAR prevents bile acid-induced hepatotoxicity[8], and regulates hepatic MDR1 expression[9], these results suggested that CAR might have similar protective functions to MDR1 in T_{eff} cells infiltrating the siLP. We confirmed that three of five *Nr1i3*-specific shRNAmirs reduced MDR1-dependent Rh123 efflux in T_{eff} cells recovered from transferred *Rag1*$^{-/-}$ mice (Extended Data Fig. 1c, d). The same clones silenced *Nr1i3* expression, as judged by ex vivo quantitative PCR (qPCR), and diminished expression of both *Abcb1a* and the signature CAR target gene *Cyp2b10*[10] (Extended Data Fig. 1e).

CAR regulates transcription as a heterodimer with retinoid X receptors (RXRs; isotypes α, β or γ)[11]. However, RXRs also dimerize with other nuclear receptors that regulate diverse aspects of T cell function in vivo[11]. Accordingly, shRNAmir-mediated depletion of RXRα predominantly reduced the persistence of T_{eff} cells in vivo (Extended Data Fig. 1f). Depletion of the CAR-related xenobiotic sensor pregnane X receptor (PXR, encoded by *Nr1i2*)[12] had little influence on either MDR1 expression or T_{eff} cell persistence (Fig. 1b, Extended Data Fig. 1f). Consistent with this, T cells from C57BL/6 (B6)-derived *Nr1i3*$^{-/-}$ mice, but not *Nr1i2*$^{-/-}$ mice, showed lower expression of MDR1 than bystander CD45.1 wild-type cells after co-transfer into *Rag1*$^{-/-}$ mice; cells lacking only CAR showed equivalently low MDR1 expression to those lacking both CAR and PXR (Extended Data Fig. 1g–i). These data implicate CAR in the regulation of mucosal T cell function in vivo.

The degree to which shRNAmir-mediated CAR depletion attenuated MDR1 expression in FVB/N wild-type T_{eff} cells after transfer into *Rag1*$^{-/-}$ mice correlated directly with the severity of weight loss that was induced by these cells (Fig. 1c, d, Extended Data Fig. 1c, d). This was consistent with our prior observation that FVB/N T cells lacking MDR1 (*Abcb1a*$^{-/-}$*Abcb1b*$^{-/-}$) induce more severe weight loss than their wild-type counterparts in reconstituted *Rag1*$^{-/-}$ mice—owing to induction of both colitis and bile acid-driven ileitis[4]—and is distinct from wild-type naive CD4^{+} T cells, which induce only colitis in immunodeficient hosts[13]. Naive T cells from B6-derived CAR-deficient mice also promoted increased weight loss and ileitis, but equivalent colitis, compared with their wild-type counterparts, after transfer into *Rag2*$^{-/-}$ mice co-housed to normalize their microflora (Fig. 1e–g). Therapeutic administration of cholestyramine (CME)[14], a bile acid-sequestering resin that prevents active bile acid reabsorption into the siLP, normalized weight loss and ileitis in CAR-deficient T cells, compared with *Rag2*$^{-/-}$ recipients of wild-type cells (Extended Data Fig. 2a, b), as did ablation of the ileal bile acid reuptake transporter ASBT (encoded by *Slc10a2*)[15], in *Rag1*$^{-/-}$ recipients (Extended Data Fig. 2c, d). Neither genetic nor pharmacological inhibition of ileal bile acid reabsorption affected the severity of colitis induced by T cell transfer (Extended Data Fig. 2b, d). These results suggest that CAR deficiency in T cells exacerbates ileitis that is not transmissible by microbiota and requires bile acid reabsorption.

To elucidate CAR-dependent transcriptional programs in T cells, we purified bystander CD45.1 wild-type and CD45.2 CAR-deficient T_{eff} cells from spleen, siLP or colon lamina propria (cLP) of co-transferred *Rag1*$^{-/-}$ mice and analysed them by RNA sequencing (RNA-seq; Fig. 2a). Gene expression in wild-type T_{eff} cells differed substantially between

spleen, siLP and cLP, whereas CAR deficiency most conspicuously altered gene expression in siLP T_{eff} cells (Fig. 2b). CAR-deficient siLP T_{eff} cells did not upregulate many 'siLP signature' genes, which are preferentially expressed in wild-type cells from siLP compared with either spleen or cLP, and ectopically expressed genes that are characteristic of wild-type T_{eff} cells from colon (Fig. 2c, d). siLP-signature genes (which encode chaperones, receptors and enzymes involved in lipid binding, transport and metabolism; for example *Apold1*, *Pex26*, *Dgkh*, *Ldlr*, *Phyhd1*, *Lclat1*) showed decreased expression in CAR-deficient compared with wild-type siLP T_{eff} cells (Fig. 2c, d), as were genes induced by CAR in mouse hepatocytes following in vivo administration of the specific CAR agonist ligand 1,4-*bis*(3,5-dichloro-2-pyridinyloxy) benzene (TC)[16] (Extended Data Fig. 3a, b). Genes that showed CAR-dependent expression in both siLP T_{eff} cells and hepatocytes were enriched for loci at which TC-inducible binding of CAR to DNA has been observed in hepatocytes by chromatin immunoprecipitation with sequencing (ChIP–seq)[17] (Extended Data Fig. 3c). These included *Abcb1a* and *Cyp2b10*, as expected, but also genes for other ABC-family transporters (for example, *Abcb4*) and cytochrome P450 enzymes (for example, *Cyp2r1*; Extended Data Fig. 3d), which suggests that CAR activates a 'hepatocyte-like' bile acid-detoxification program in siLP T_{eff} cells. There was less accumulation of CAR-deficient T_{eff} cells than of wild-type bystanders in the siLP of *Rag1*$^{-/-}$ recipient mice initially, and in all tissues later (Extended Data Fig. 4a–c); ablation of ASBT-dependent bile acid reabsorption in *Rag1*$^{-/-}$ recipients tended to minimize this phenotype (Extended Data Fig. 4d–f).

To test whether CAR also regulates small intestine-associated T cell function in humans, we analysed its expression and function in T cell subsets from healthy adult peripheral blood that are most likely to have recirculated from the siLP. Between 1 and 5% of circulating T_{eff} cells expressed the full combination of siLP-homing receptors, α4β7 integrin and CCR9[18] ($\alpha4^+\beta7^+CCR9^+$), whereas naive T cells that lack gut-homing potential did not (Extended Data Fig. 5a–c). Fewer $CD25^+$ T regulatory (T_{reg}) cells than T_{eff} cells expressed these receptors (Extended Data Fig. 5a–c), which suggests that T_{reg} cells may be more efficiently retained in the siLP than T_{eff} cells. Indeed, siLP-linked $\alpha4^+\beta7^+CCR9^+$ T_{eff} cells displayed elevated expression of *ABCB1*, *NR1I3* and *CYP2B6* (orthologue of mouse *Cyp2b10*[19]) compared with naive, T_{reg} or T_{eff} cells that lacked one or more siLP-homing receptors (Extended Data Fig. 5d–f). Furthermore, only $\alpha4^+\beta7^+CCR9^+$ T_{eff} cells responded to ex vivo treatment with the human CAR agonist 6-(4-chlorophenyl)imidazo[2,1-b] [1,3]thiazole-5-carbaldehyde O-(3,4-dichlorobenzyl) oxime (CITCO)[18] by upregulating *CYP2B6* and *ABCB1* (Extended Data Fig. 5g, h). $CCR6^+CXCR3^{hi}CCR4^{lo}$ 'T helper (T_H) 17.1' cells, which possess both T_H17 and T_H1 effector functions and high MDR1 expression[20], were enriched among total $\alpha4^+\beta7^+CCR9^+$ T_{eff} cells (Extended Data Fig. 5i–l). However, MDR1 expression was higher in $\alpha4^+\beta7^+CCR9^+$ $T_H17.1$ cells than in their counterparts lacking one or more siLP-homing receptors (Extended Data Fig. 5m, n). The same was true for T_H17 ($CCR6^+CXCR3^{lo}CCR4^{hi}$) and T_H1 ($CCR6^-CXCR3^{hi}CCR4^{lo}$) cells. These data suggest that CAR preferentially operates in both mouse and human small intestinal T_{eff} cells.

Preferential CAR function in siLP T_{eff} cells could involve activation by local metabolites. Consistent with this idea, gallbladder bile or sterile-filtered soluble small intestine lumen content (siLC) from wild-type B6 mice—but not colon lumen content (cLC) or serum — induced upregulation of *Abcb1a* and *Cyp2b10* in ex vivo-stimulated wild-type, but

not CAR-deficient, T_{eff} cells from recipient *Rag1*$^{-/-}$ mice (Fig. 2e, Extended Data Fig. 6a). CAR-dependent gene expression in this ex vivo culture system was also induced by TC, inhibited by the CAR inverse agonist 5α-androstan-3β-ol[8], and unaffected by the PXR agonist 5-pregnen-3β-ol-20-one-16α-carbonitrile (PCN)[12] (Extended Data Fig. 6b, c). Bile and siLC concentrations that enhanced CAR-dependent gene expression in T_{eff} cells also promoted recruitment of a PGC1α co-activator peptide to recombinant CAR–RXRα ligand-binding domain (LBD) heterodimers, but not to RXRα LBD homodimers, in time-resolved fluorescence resonance energy transfer (TR-FRET) experiments (Fig. 2f, g, Extended Data Fig. 7a, b). As CAR is thought to indirectly sense, but not directly bind, major bile acid species[21], we reasoned that biliary metabolites other than bile acids (phospholipids, cholesterol, fatty acids and bilirubin)[1] might activate the CAR LBD. Indeed, siLC pre-treated with CME to deplete free bile acids[4] retained the ability to activate CAR–RXRα LBD heterodimers (Extended Data Fig. 7c). Furthermore, no major bile acid species activated CAR–RXRα LBD heterodimers in TR-FRET experiments, or stimulated CAR-dependent gene expression in ex vivo-cultured T_{eff} cells (Extended Data Fig. 7d and data not shown). siLC from germ-free mice also activated CAR– RXRα LBD heterodimers (Extended Data Fig. 7c and data not shown). These data suggest that host-derived, non-bile acid constituents of bile might contribute to the enhanced transcriptional activity of CAR in siLP T_{eff} cells.

To further investigate the immunoregulatory functions of CAR, we examined its control of gene expression associated with major pro- and anti-inflammatory T_H cell lineages. Genes expressed selectively in type 1 regulatory (T_R1) cells[22]—a FOXP3$^-$IL-10$^+$ subset known for suppressing mucosal inflammation in humans and mice[23]—were reduced in CAR-deficient compared with wild-type siLP T_{eff} cells (Fig. 3a–c). Conversely, genes characteristic of pro-inflammatory IL-17-secreting (T_H17) cells[24] were increased in siLP T_{eff} cells that lacked CAR (Fig. 3b). In line with these signatures, CAR-deficient T_{eff} cells showed inefficient expression of both *Thy1.1* as an *Il10* reporter (from 10BiT reporter mice[25]; Fig. 3d) and endogenous IL-10 protein (Extended Data Fig. 8a–e), after transfer into *Rag1*$^{-/-}$ mice. Reduced *Il10* expression in T_{eff} cells lacking CAR paralleled their accumulation as RORγt$^+$IL-17A$^-$ 'poised' T_H17 cells[26,27] in siLP (Extended Data Fig. 8f, g). *Il10*$^{-/-}$ T cells replete for CAR recapitulated this poised T_H17 cell phenotype in siLP (Extended Data Fig. 8h, i), which suggests that CAR might reciprocally regulate T_R1 and T_H17 cell development in the siLP through the induction of IL-10. TC, or bile or siLC from wild-type mice, promoted the upregulation of *Il10* in ex vivo-stimulated wild-type, but not CAR-deficient, T_{eff} cells (Fig. 3e, Extended Data Fig. 6), akin to *Abcb1a* and *Cyp2b10* (Fig. 2e).

CAR-dependent IL-10 expression in T cell-reconstituted *Rag1*$^{-/-}$ mice was transient—peaking two weeks after donor T cell engraftment and waning thereafter—and followed the kinetics of both T_{eff} cell infiltration into the siLP and ex vivo *Nr1i3*, *Abcb1a* and *Cyp2b10* gene expression (Extended Data Fig. 9a–c). This suggested that CAR activity in T_{eff} cells might be increased in response to mucosal inflammation, analogous to T_R1 cell dynamics in vivo[28]. Using an independent approach to induce intestinal inflammation in wild-type or CAR-deficient mice—injection of soluble anti-CD3[23]—we confirmed that CAR was required for anti-CD3 (inflammation)-induced upregulation of IL-10 by endogenous effector and regulatory T cell subsets in the siLP, but not the spleen, and was dispensable for

steady-state IL-10 expression in T cells from unmanipulated mice (Extended Data Fig. 9d–f).

To model CAR-dependent T_R1 cell function in vitro, we tested CAR expression and function in naive $CD4^+$ T cells that were activated and expanded in culture conditions that induce the differentiation of $FOXP3^-IL\text{-}10^+$ 'T_R1-like' cells. Combining IL-27—a cytokine that promotes STAT3-dependent IL-10 expression[22]—with the synthetic corticosteroid dexamethasone (Dex)[29] induced expression of *Nr1i3* and IL-10, but not FOXP3, in activated T cells (Fig. 3f–h and data not shown). Loss of CAR impaired production of IL-10 by IL-27 plus Dex-elicited T_R1-like cells (Fig. 3g, h). By contrast, expression of *Nr1i3* remained low during the in vitro development of other effector (for example, T_H1, T_H2, T_H17) or $FOXP3^+$-induced T_{reg} lineages, and CAR ablation had little impact on the development or function of these cells (Supplementary Table 3). These results suggest that CAR is essential for regulation of *Il10* in T_R1 cells, which may synergize with CAR-dependent bile acid detoxification to enforce small bowel immune homeostasis.

Finally, we reasoned that if CAR deficiency in T_{eff} cells exacerbates bile acid-driven small bowel inflammation, pharmacological CAR activation might protect against it. A single administration of the CAR agonist TC to $Rag1^{-/-}$ mice reconstituted with mixtures of CD45.1 wild-type and CD45.2 CAR-deficient T cells induced upregulation of *Abcb1a*, *Cyp2b10* and *Il10* in wild-type, but not CAR-deficient, T_{eff} cells within 72 h (Fig. 4a). Weekly TC administration reduced ileitis, but not colitis, in $Rag2^{-/-}$ mice reconstituted with only wild-type T cells and fed a standard 0.2% cholic acid-supplemented diet to increase the size of the circulating bile acid pool and promote small bowel injury[8,12] (Fig. 4b, c). Feeding with cholic acid increased morbidity in $Rag2^{-/-}$ mice that received wild-type T cells, but had no obvious effects on $Rag2^{-/-}$ mice that did not undergo T cell transfer (Fig. 4b). The therapeutic effects of TC were abolished in cholic acid-fed $Rag2^{-/-}$ mice reconstituted with CAR-deficient T cells (Extended Data Fig. 10), which suggests that bile acid supplementation promotes experimental ileitis, whereas CAR activation in T cells suppresses it.

Enterohepatic circulation establishes a marked concentration gradient of bile acids in the small intestine (millimolar) and colon (micromolar), which opposes that of bacteria and bacterial metabolites[1]. Although antigens from the enteric flora prime both pro- and anti-inflammatory T cell responses across the intestinal tract, the specific requirement for CAR function in siLP T_{eff} cells—defined here in an in vivo screen, and relative to other nuclear receptors with known regulatory functions in the colon (for example, the vitamin D receptor)[30]—suggests important distinctions between the immunoregulatory microenvironments of the small and large intestines. Opposing gradients of bile and bacteria in the small and large intestines could be sensed by distinct sets of nuclear receptors in mucosal lymphocytes to instruct compartmentalized regulatory functions. Microbe-induced $FOXP3^+$ T_{reg} cell development is most prominent in the colon and involves the vitamin D receptor[30], for example, whereas we show here that CAR senses enterohepatically circulating host metabolites in the small intestine to counter bile acid toxicity and promote $FOXP3^-$ T_R1 cell function (Fig. 4d). Important questions remain about the interplay between CAR and biliary metabolites, the identity and function of transcriptional targets

of CAR in T cells, and the role of CAR in other, spontaneous models of small bowel Crohn's disease, but our results suggest that activation of CAR could be a therapeutic target in Crohn's disease and provide insight into lymphocyte specialization across the intestinal tract.

Methods

Mice

C57BL/6 (B6)-derived wild-type (stock no: 000664), CD45.1 (stock no: 002014), *Rag1*$^{-/-}$ (stock no: 002216), *Rag2*$^{-/-}$ (stock no: 008449) and *Il10*$^{-/-}$ (stock no: 002251) mice were purchased from The Jackson Laboratory. Wild-type FVB/N mice were purchased from Taconic. B6-derived *Nr1i2*$^{-/-}$, *Nr1i3*$^{-/-}$ and *Nri12*$^{-/-}$*Nr1i3*$^{-/-}$ mice were provided by D. Moore (Baylor College of Medicine, BCM). FVB/N-derived *Rag1*$^{-/-}$ mice were a gift from Dr. Allan Bieber (Mayo Clinic, Rochester, MN). B6-derived BAC *Il10*-Thy1.1 transgenic reporter (10BiT) mice were provided by C. Weaver (University of Alabama-Birmingham, UAB) and have been described previously[25]. B6-derived *Rag1*$^{-/-}$ mice were crossed with *Slc10a2*$^{-/-}$ mice (gift from Dr. Paul Dawson, Emory University) in the Sundrud laboratory to generate *Rag1*$^{-/-}$ mice lacking the ASBT transporter as described[4]. Lumen contents (colon, small intestine) were collected (see below) from specific pathogen-free (SPF) or germ-free wild-type B6 mice housed at the University of Alabama-Birmingham (UAB; courtesy of C.T.W.). All breeding and experimental use of animals was conducted in accordance with protocols approved by IACUC committees at Scripps Florida, BCM or UAB.

Human blood samples

Human blood samples were collected and analysed in accordance with protocols approved by Institutional Review Boards at Scripps Florida and OneBlood (Orlando, Florida). Blood was obtained following informed written consent, and consenting volunteers willingly shared their clinical history and demographic information before phlebotomy. Institutional Review Boards at OneBlood and Scripps Florida approved all procedures and forms used in obtaining informed consent, and all documentation for consenting volunteers is stored at OneBlood.

CD4$^+$ T cell isolation and culture

Purified CD4$^+$CD25$^-$ T cells were magnetically isolated from spleen and peripheral lymph node mononuclear cells using an EasySep magnetic T cell negative isolation kit (Stem Cell Technologies, Inc.) with the addition of a biotin anti-mouse CD25 antibody (0.5 μg/ml; BioLegend). Magnetically enriched CD4$^+$ T cells were cultured in Dulbecco's modified Eagle's medium (DMEM) supplemented with 10% heat-inactivated fetal bovine serum (BioFluids), 2 mM L-glutamine (Gibco), 50 μM 2-mercaptoethanol (Amresco), 1% MEM vitamin solution (Gibco), 1% MEM non-essential amino acids solution (Gibco), 1% sodium pyruvate (Gibco), 1% arg/asp/folic acid (Gibco), 1% HEPES (Gibco), 0.1% gentamicin (Gibco) and 100 U/ml Pen-Strep (Gibco). For *Rag1*$^{-/-}$ transfer experiments, magnetically enriched CD4$^+$CD25$^-$ T cells were FACS-sorted to obtain pure naive T cells (CD3$^+$CD4$^+$CD25$^-$CD62L^{hi}CD44^{lo}). For ex vivo isolation of mononuclear cells

from tissues of T cell-reconstituted RAG-deficient mice, single-cell suspensions were prepared from spleen, peripheral lymph nodes, or mesenteric lymph nodes (MLNs) by mechanical disruption and passing through 70-μm nylon filters (BD Biosciences). For intestinal tissues, small intestines and colons were removed, rinsed thoroughly with PBS to remove faecal contents, and opened longitudinally. Tissues were incubated for 30 min at room temperature in DMEM without phenol red (Genesee Scientific) plus 0.15% DTT (Sigma-Aldrich) to eliminate the mucus layer. After washing with medium, intestines were incubated for 30 min at room temperature in medium containing 1 mM EDTA (Amresco) to remove the epithelium. Intestinal tissue was digested in medium containing 0.25 mg/ml liberase TL(Roche) and 10U/ml RNase-free DNaseI(Roche) for 15–35 min at 37 °C. Lymphocyte fractions were obtained by 70/30% Percoll density gradient centrifugation (Sigma-Aldrich). Mononuclear cells were washed in complete T cell medium and resuspended for downstream FACS analysis or sorting.

Naive CD4$^+$ T cell activation and polarization.—Magnetically enriched CD4$^+$CD25$^-$ T cells were seeded (at 4×10^5 cells/cm^2 and 1×10^6 cells/ml) in 96- or 24-well flat-bottom plates pre-coated for 2 h at 37 °C with goat-anti-hamster whole IgG (50 μg/ml; Invitrogen). Activation was induced by adding hamster-anti-mouse CD3ε (0.3 or 1 μg/ml; BioLegend) and hamster-anti-mouse CD28 (0.25 or 0.5 μg/ml; BioXcell). After 48 h, cells were removed from coated wells and re-cultured at 1×10^6 cells/ml in medium with or without 10 U/ml recombinant human IL-2 (rhIL-2) (NIH Biorepository), depending on the experiment (see below). For polarization studies, cells were activated in the presence of the following sets of cytokines and/or neutralizing antibodies (all from R&D Systems): T_H0: medium alone; T_H1: recombinant human (rh)IL-12 (5 ng/ml) plus anti-mouse IL-4 (5 μg/ml); T_H2: rhIL-4 (10 ng/ml) plus anti-mouse IFNγ (5 μg/ml); non-pathogenic (np)T_H17: recombinant mouse (rm)IL-6 (40 ng/ml) plus rhTGFβ1 (1 ng/ml), anti-mouse IFNγ (5 μg/ml) and anti-mouse IL-4 (5 μg/ml); pathogenic (p)T_H17: rmIL-6 (40 ng/ml) plus rhTGFβ1 (1 ng/ml), rhIL-23 (10 ng/ml) anti-mouse IFNγ (5 μg/ml) and anti-mouse IL-4 (5 μg/ml); induced T regulatory (iT_{reg}): rhTGFβ1 (5 ng/ml) plus rhIL-2 (10 U/ml), anti-mouse IFNγ (5 μg/ml) and anti-mouse IL-4 (5 μg/ml). For T_R1 cultures, cells were activated in the presence of rhIL-27 (100 ng/ml) and/or dexamethasone (100 nM; Sigma-Aldrich). Cytokine, antibodies and/or dexamethasone were added at the time of activation (day 0), and re-added to expansion medium between days 2 and 4 of culture. Cells were analysed for intracellular expression of transcription factors and/or cytokines, to confirm polarization, on day 4 after re-stimulation with phorbol 12-myrisate 13-acetate (PMA; 10 nM; Life Technologies) and ionomycin (1 μM; Sigma-Aldrich) for 3–4 h in the presence of brefeldin A (BFA; 10 μg/ml; Life Technologies).

Ex vivo stimulation of FACS-sorted T_{eff} cells from reconstituted *Rag1*$^{-/-}$ mice.—Thirty-thousand CD45.1 (wild-type) or CD45.2 (*Nr1i3*$^{-/-}$) cells that had been FACS-purified from spleens of B6.*Rag1*$^{-/-}$ mice 2–3 weeks after naive T cell transfer were activated in round-bottom 96-well plates with mouse anti-CD3/anti-CD28 T cell expander beads (1 bead per cell; Life Technologies) in complete medium containing 10 U/ml rhIL-2 for 24 h in the presence or absence of synthetic or endogenous CAR agonists (see ‘Compounds and tissue extracts‘).

Retroviral plasmids and transductions

shRNAmirs against mouse nuclear receptors were purchased (TransOMIC) or custom synthesized using the shERWOOD algorithm[31]. For cloning into an ametrine-expressing mouse retroviral vector (LMPd) containing the enhanced miR-30 (miR-E) cassette[6,32], shRNAmirs were PCR amplified using forward (5′-AGAAGGCTCGAGAAGGTATATTGC-3′) and reverse (5′-GCTCGAATTCTAGCCCCTTGAAGTC CGAGG-3′) primers containing XhoI and EcoR1 restriction sites, respectively. All retroviral constructs were confirmed by sequencing before use in cell culture experiments. Retroviral particles were produced by transfection of Platinum E (PLAT-E) cells with the TransIT-LT1 transfection reagent (Mirus) in Opti-MEM I reduced serum medium. Viral supernatants containing 10 μg/ml polybrene were used to transduce $CD4^+CD25^-$ T cells 24 h after activation (anti-CD3/anti-CD28; as above). Transductions were enhanced by centrifugation at 2,000 rpm for 1 h at room temperature, and incubation at 37 °C until 48 h after activation. Transduced cells were expanded in complete medium containing 10 U/ml rhIL-2.

Cell lines

PLAT-E cells, derived from HEK-293 human embryonic kidney fibroblasts and engineered for improved retroviral packaging efficiency, were provided by M. Pipkin (Scripps Florida). All cell lines were tested to be mycoplasma free, and cultured in DMEM plus 10% FBS, 2 mM L-glutamine, 50 μM 2-mercaptoethanol, 1% HEPES, 0.1% gentamicin and 100 U/ml Pen-Strep.

T cell transfer colitis

For experiments using B6-derived wild-type or CAR-deficient (*Nr1i3*$^{-/-}$) T cells, 0.5×10^6 FACS-sorted naive T cells (sorted as $CD4^+CD25^-CD62L^{hi}CD44^{lo}$ at Scripps Florida; $CD4^+CD45RB^{hi}$ at BCM) were injected intraperitoneally (i.p.) into syngeneic *Rag1*$^{-/-}$ (at Scripps Florida) or *Rag2*$^{-/-}$ (at BCM) recipients and analysed between 2 and 6 weeks after transfer. For mixed congenic T cell transfers, FACS-purified naive T cells ($CD4^+CD25^-CD62L^{hi}CD44^{lo}$) from CD45.1 wild-type and CD45.2 CAR-deficient (*Nr1i3*$^{-/-}$), PXR-deficient (*Nr1i2*$^{-/-}$), CAR- and PXR-deficient (*Nri12*$^{-/-}$*Nr1i3*$^{-/-}$) or *Il10*$^{-/-}$ mice were mixed in a 1:1 ratio and transferred together (0.5×10^6 total cells). For transfers of shRNAmir-expressing T cells, magnetically enriched $CD4^+CD25^-$ T cells from FVB/N wild-type mice, activated and transduced as above, were expanded until day 5 in medium containing rhIL-2 and transferred into syngeneic *Rag1*$^{-/-}$ mice (0.5×10^6 total cells). All *Rag1*$^{-/-}$ recipients were weighed immediately before T cell transfer to determine baseline weight, and then weighed twice weekly after T cell transfer for the duration of the experiment. Mouse chow diets containing 2% cholestyramine (CME) (Sigma-Aldrich) or 0.2% cholic acid (Sigma-Aldrich) and control diets were custom made (Teklad Envigo, Madison, WI) and fed to mice as follows: CME-supplemented diets were started 3 weeks after T cell transfer and continued for 3 weeks; cholic acid diet was started within 3 days after T cell transfer and continued for 6 weeks (or until mice died). TC (Sigma-Aldrich) was initially reconstituted in sterile DMSO, stored at −20 °C, and diluted in sterile saline and sonicated immediately before injections. We injected 3 mg/kg TC i.p. weekly as indicated.

Transferred *Rag1*$^{-/-}$ or *Rag2*$^{-/-}$ mice were killed when they had lost 20% of pre-transfer baseline weight. All *Rag*$^{-/-}$ mice that received different donor T cell genotypes were co-housed to normalize microflora exposure.

Anti-CD3-induced intestinal injury

Wild-type (B6) or CAR-deficient (B6.*Nr1i3*$^{-/-}$) mice were injected i.p. with 15 μg of soluble, ultra-LEAF purified anti-CD3 (clone: 145–2C11) or IgG isotype control (clone: HTK888) (BioLegend) twice over 48 h. Animals were killed and T cells analysed 4 h after the second injection.

Histology

Colon(proximal, distal) orsmall intestine (proximal, mid, distal/ileum) sections (~1 cm) were cut from killed *Rag1*$^{-/-}$ or *Rag2*$^{-/-}$ mice 6 weeks after T cell transfer. In some experiments, 10-cm segments of distal small intestine and whole colon were dissected from mice and fixed intact. All tissues were fixed in 10% neutral buffered formalin, embedded into paraffin blocks, cut for slides at 4–5 μm, and stained with H&E. H&E-stained sections were analysed and scored blindly by a pathologist with gastrointestinal expertise using an Olympus BX41 microscope and imaged using an Olympus DP71 camera. Colons and ilea were histologically graded for inflammation severity using a combination of previously reported grading models[33,34]. The first scheme[33] grades five different descriptors which include crypt architecture (normal, 0; severe crypt distortion with loss of entire crypts, 3), degree of inflammatory cell infiltration (normal, 0; dense inflammatory infiltrate, 3), muscle thickening (base of crypt sits on the muscularis mucosae, 0; marked muscle thickening present, 3), goblet cell depletion (absent, 0; present, 1) and crypt abscess (absent, 0; present, 1). The histological damage score is the sum of each individual score.

Flow cytometry

Cell surface and intracellular FACS stains were performed at 4 °C for 30 min, washed with phosphate buffered saline (PBS) and acquired on a flow cytometer. Analysis of Rh123 efflux was performed as described[4]. Background Rh123 efflux was determined by the addition of the MDR1 antagonist elacridar (10 nM) to Rh123-labelled cells before the 37 °C efflux step. Anti-mouse antibodies used for FACS analysis included: Alexa Fluor 700 anti-CD45, APC anti-CD45.1, BV711 anti-CD4, BV510 anti-CD25, BV650 anti-CD3, Percp-Cy5.5 anti-CD62L, PE-CY7 anti-CD44, BV605 anti-CD62L, PE anti-α4β7, Alexa Fluor700 anti-CD4, FITC anti-CD44, BV421 anti-CD44, e450 anti FOXP3, BV605 anti-TNF, Percp-Cy5.5 anti-IL-17a, BV711 anti-INFγ, PE anti-IL-4, PE-CY7 anti-IL-10, PE anti-Thy1.1, FITC anti-CD3, Percp-Cy5.5 anti-Thy1.1, PE anti-CD3, PE anti-TCRβ, APC anti-INFγ, FITC anti-CD45.2, PE anti-α4β7, Alexa Fluor700 anti-CD45.1, PE-CY7 anti-CD45.1 (from BioLegend); and BUV395 anti-CD3, PE-CF594 anti-CD25, FITC anti-Ki-67, PE-CF594 anti-RORγt, FITC anti-CD4, PE anti-CD45RB (from BD). Anti-human antibodies used for FACS analysis included: APC anti-CD3, PE anti-CD4, PE-Cy7 anti-CD45RO, BV711 anti-CD49a (integrin α4), APC-Fire 750 anti-integrin β7, BV421 anti-CCR9, and Percp-Cy5.5 anti-CCR7, BV605 anti-CCR2, PE anti-CRTH2, PE anti-CCR10, PE-Cy7 anti-CCR4, Percp-Cy5.5 anti-CXCR3, APC anti-CCR6, BV605 anti-CD4, PE-CF594 anti-CD25 (from BD). Vital dyes include: fixable viability eFluor 506, eFluor 660 and eFluor 780 (all from

eBioscience). Rh123 and elacridar were purchased from Sigma-Aldrich. All FACS data were acquired on LSRII or FACSCanto II instruments (BD), and analysed using FlowJo 9.9.6 or FlowJo 10.7.1 software (TreeStar, Inc.).

Cell sorting

Cells stained with cell-surface antibodies, as above, were passed through 70-μm nylon filters, resuspended in PBS plus 1% serum, and sorted on a FACS AriaII machine (BD Biosciences). Sorted cells were collected in serum-coated tubes containing PBS plus 50% serum. Gates used to sort MDR1$^{+/-}$ T cells, based on Rh123 efflux, were set using background Rh123 efflux in elacridar-treated cells. For human T cell sorts, peripheral blood mononuclear cells (PBMCs) were isolated using Ficoll-Plaque PLUS (GE Healthcare) from 25 ml of enriched buffy coats (OneBlood). CD4$^+$ T cells were enriched using the human total CD4 T cell Negative Isolation kit (EasySep), followed by enrichment of either effector/memory T cells (Human Memory CD4 T cell Enrichment kit; EasySep) or T_{reg} cells (Human CD4$^+$CD127^{lo}CD49d$^-$ T_{reg} Enrichment Kit; EasySep) (all from StemCell Technologies). Enriched cells were stained with anti-human FACS antibodies (listed above) for 20 min on ice. Stained cells were filtered through sterile 40-μM mesh filters and re-suspended in PBS with 5% FBS and 0.1% DNase. In cases where RNA was isolated after sorting, 100,000 cells were sorted into 200 μl PBS with 1 μM DTT and 5 μl RNase Inhibitor Cocktail (Takara); for ex vivo culture experiments, 0.4–1.2 × 10^6 cells were sorted into complete T cell medium.

Pooled in vivo shRNAmir screen

Two independent pooled screens were performed. In brief, PLAT-E cells were cultured in 96-well plates with 5 × 10^4 per well in 100 μl complete medium and transfected as described above. Magnetically enriched CD4$^+$CD25$^-$ T cells from spleens of 7- to 8-week-old female FVB/N mice were activated with anti-CD3 and anti-CD28 in 96-well plates and transduced 24 h after activation. The transduction efficiency of each individual shRNAmir was determined on day 4. On day 5, all wells were pooled and transduced (ametrine$^+$) cells were FACS-sorted and adoptively transferred (i.p.) into 10 FVB/N.*Rag1*$^{-/-}$ mice. An aliquot of sorted cells was saved for genomic DNA isolation and used for input reference. Six weeks after transfer, live (viability dye$^-$) transduced (ametrine$^+$) Rh123^{hi} (MDR1$^-$) or Rh123^{lo} (MDR1$^+$) effector/memory T cells (T_{eff}; CD4$^+$CD25$^-$CD62L^{lo}CD44^{hi}) were FACS-sorted from the spleen or small intestine lamina propria of FVB/N.*Rag1*$^{-/-}$ recipients. High-quality genomic DNA was isolated using PureLink Genomic DNA Mini Kit (Invitrogen) and 100 ng DNA was used for library preparation. gDNA derived from transduced and sorted T cells was quantified with Qubit DNA assay. We used 75 ng gDNA as a template in duplicate reactions to add the Ion adaptor sequences and barcodes. On the basis of previous data, we used 28 cycles of PCR to amplify the libraries using primers with Ion P1 miR30 loop sequence (5′-CCTCTCTATGGGCAGTCGGTGATTACATCTGTGGCTTC-ACTA-3′) and Ion A miR-30 (5′-CCATCTCATCCCTGCGTGT CTCCGACTCAG XXXXXXXXXX-GCTCGAGAAGGTATATTGCT-3′) sequences. The miR-30 loop (PI) and miR-30 (A) annealing sequences are underlined. The IonXpress 10-nt barcode is depicted with a string of Xs. Sequencing libraries were purified with 1.6× Ampure XP beads (Beckman Coulter), quantified with Qubit DNA HS assay (Invitrogen), and visualized on the Agilent 2100

Bioanalyzer (Agilent Technologies, Inc.). Individually barcoded libraries were pooled at equimolar ratios and templated on to Ion spheres at 50 pM loading concentration using the Ion Chef (Life Technologies) with the Ion PI IC 200 kit. The templated Ion spheres (ISPs) were quantified using AlexaFluor sequence-specific probes provided in the Ion Sphere quality control kit (Life Technologies). The per cent templated ISPs within 10–20% were taken forward to loading on the Ion PI V2 chips and then run on the Ion Proton with 200-bp reads. Libraries were sequenced using the Ion Torrent technology from Life Technologies following the manufacturer's instructions. Sequencing reads were aligned to the reference library using BLAST with default settings and raw counts were normalized with DESeq2. Normalized reads of shRNAmirs displaying ≤10-fold change between input and ex vivo spleen samples were considered for downstream analysis. The relative enrichment or depletion of shRNAmirs was determined using median $\log_2$ fold changes in mean shRNAmir abundances in $MDR1^{hi}$ versus $MDR1^{lo}$ T_{eff} cells. Mean shRNAmir abundances for each gene target were determined in two independent screens, each using cells recovered from pools of 10 spleens and siLP of transferred FVB/N.*Rag1*$^{-/-}$ mice.

Compounds and tissue extracts

We added 10 or 20 μM 1,4-bis-[2-(3,5-dichloropyridyloxy)]benzene, 3,3′,5,5′-tetrachloro-1,4-bis(pyridyloxy) benzene (TC), 10 μM 5α-androstan-3β-ol (And), 10μM 5-pregnen-3β-ol-20-one-16α-carbonitrile (PCN) (all from Sigma-Aldrich), or serum, bile (from gallbladder), sterile soluble siLC, or sterile soluble cLC from wild-type (B6) mice to mouse naive T cells or T_{eff} cells stimulated with anti-CD3/anti-CD28 antibodies as above. For preparation of mouse tissue extracts, mouse siLC or cLC was extracted from whole tissue into a sterile tube. Contents were weighed, diluted with an equal volume of sterile PBS and vortexed vigorously for 30 s, and then supernatants were collected after sequential centrifugation steps: (i) 10 min at 930*g*; and (ii) 10 min at 16*g*. Cleared supernatants were finally sterile filtered using 0.22-μm filters and aliquots were frozen at −20 °C. Serum was collected in EDTA-coated tubes and centrifuged for 5 min at 2.4*g*. Owing to the small sample size, serum and gallbladder bile were used directly without filter sterilization after harvesting. Equal volumes of sterile vehicle (DMSO for TC, And; ethanol for PCN; PBS for sterile mouse content) served as negative controls. For human T cell culture experiments, healthy adult donor PBMCs were FACS-sorted for the following subsets: (i) naive $CD4^+$ T cells ($CD4^+$ $CD25^-CD45RO^-CCR7^{hi}$); (ii) T_{reg} cells ($CD4^+CD25^{hi}$); (iii) $\alpha4^-CCR9^-$ T_{eff} cells ($CD4^+CD25^-CD45RO^+$); and (iv) $\alpha4^+CCR9^+$ T_{eff} cells ($CD4^+CD25^-$ $CD45RO^+$). Note that all $\alpha4^-CCR9^-$ T_{eff} cells are integrin $\beta7^-$ and all $\alpha4^+CCR9^+$ T_{eff} cells are integrin $\beta7^+$. For all subsets, 30,000 purified cells were stimulated in round-bottom 96-well plates with human anti-CD3/anti-CD28 T cell expander beads (1 bead per cell; ThermoFisher) in complete medium containing 10 U/ml rhIL-2 with or without 10 or 20 μM 6-(4-chlorophenyl)imidazo[2,1-b][1,3]thiazole-5-carbaldehyde O-(3,4-dichlorobenzyl)oxime (CITCO) (Sigma-Aldrich); an equal volume of DMSO served as the negative control.

qPCR

RNA was isolated from cultured or ex vivo-isolated cells using RNeasy Mini columns with on-column DNase treatment (Qiagen); RNA was used to synthesize cDNA with

a high capacity cDNA reverse transcription kit (Life Technologies). Taqman qPCR was performed on a StepOnePlus real-time PCR instrument (Life Technologies/Applied Biosystems) using commercial Taqman primer/probe sets (Life Technologies). Probes for mouse genes included: *Abcb1a* (Mm00607939_s1), *Nr1i3* (Mm01283981_g1), *Cyp2b10* (Mm01972453_s1), *Il10* (Mm01288386_m1) and *Actb (Mm00607939_s1)*; probes for human genes included: *NR1I3* (Hs00901571_m1), *ABCB1* (Hs00184500_m1), *CYP2B6* (Hs04183483), *IL10* (Hs00961622_m1), and *ACTB* (Hs0160665_g1).

Bioinformatics

ChIP–seq.—Raw sequencing reads for CAR were downloaded from the Gene Expression Omnibus (GSE112199)[16], aligned to USC mm10 with Bowtie2[35] and analysed to identify significant DNA-binding peaks (base settings; FDR q value cutoff < 0.05) with MACS2[36]. Read files for biological replicates were merged and the resulting bigwig files were visualized with Integrated Genome Viewer (IGV)[37]. Peaks were filtered to remove reads with alternative annotations, mitochondrial DNA, or blacklist regions in R using GenomeInfoDb and GenomicRanges packages.

RNA-seq.—Next-generation RNA-seq was performed on FACS-sorted B6 wild-type and CAR-deficient T_{eff} cells (viability dye^{-}CD45^{+}CD3^{+}CD4^{+} CD25^{-}CD44^{hi}) from spleen, small intestinal lamina propria, and colon lamina propria of *Rag1*$^{-/-}$ mice injected 3 weeks earlier with 1:1 congenic mixtures of CD45.1 wild-type and CD45.2 *Nr1i3*$^{-/-}$ naive T cells. Approximately 500 sorted cells were processed directly to generate cDNA using the Clontech SMART-Seq v4 Ultra Low Input Kit (Clontech, Inc.) on three biologically independent replicates. The generated cDNA was size-selected using beads to enrich for fragments >400 bp. The enriched cDNA was converted to Illumina-compatible libraries using the NEBNext Ultra II DNA kit (New England Biolabs, Inc.) using 1 ng input. Final libraries were validated on the Agilent 2100 bioanalyzer DNA chips and quantified on the Qubit 2.0 fluorometer (Invitrogen, Life Technologies). Barcoded libraries were pooled at equimolar ratios and sequenced using single-end 75-bp reads on a NextSeq 500 instrument (Illumina). Raw sequencing reads (fastq files) were mapped to the mm10 transcriptome and transcript abundance—as transcripts per million (TPM)—were quantified using Salmon[38]. Ensemble gene IDs were converted to gene symbols using R package biomaRT. PCA was performed and projected in R-studio. Differentially expressed genes (DEGs) were determined using DESeq2, using $P < 0.05$ cutoffs. DEG datasets were loaded into R using DOSE for gene ontology (GO) term enrichment analysis, which was performed using the R package, ClusterProfiler. $\log_2$[fold change] was used as the ranking metric to generate input-ranked lists for gene set enrichment analysis (GSEA)[39,40] (https://www.gsea-msigdb.org/gsea/index.jsp); these genes were compared against both customized and curated gene sets (the latter from the Molecular Signature Database (MSigDB)) for enrichment—quantified as NES—and visualized using the ggplot2 package in R. For GSEA summary plots (Figs. 2d, 3b, Extended Data Fig. 3b), circle sizes indicate significance ($-\log_{10}$[nominal P values]). Red–blue colouring indicates enrichment within genes that were up- or downregulated, respectively, in CAR-deficient versus wild-type T_{eff} cells, based on the positive or negative portion of the distribution corresponding to the sign of the observed NES. Differentially expressed genes of wild-type T_{eff} cells from spleen, siLP, or cLP, determined by DESeq2,

were used to generate tissue-specific T_{eff} gene sets: (i) up in B6 spleen T_{eff}, genes expressed higher in spleen than in either siLP or cLP wild-type T_{eff} cells; (ii) up in B6 siLP T_{eff}, genes expressed higher in siLP than in either spleen or cLP wild-type T_{eff} cells; and (iii) up in B6 cLP T_{eff}, genes expressed higher in cLP than in either spleen or siLP wild-type T_{eff} cells. RNA-seq data for pharmacological activation of CAR or PXR in hepatocytes in vivo from mice treated with the CAR agonist TCPOBOP (TC), the PXR agonist PCN, or vehicle (corn oil) (GSE104734)[15] were analysed to generate additional gene sets: (iv) up in Hep + TC, genes expressed higher in hepatocytes from TC-than from either PCN- or corn oil-treated mice; and (v) up in Hep + PCN, genes expressed higher in hepatocytes from PCN-than from either TC- or corn oil-treated mice. Differential gene expression between in vitro-differentiated T_R1 (GSE92940)[21] and T_H17 cells (GSE21670)[41] was determined using the Limma package in R[42] (for microarray data) to generate the gene sets: (vi) T_R1 signature, genes expressed higher in in vitro-polarized T_R1 cells than in non-polarizing (T_H0) conditions; and (vii) T_H17 signature, genes expressed higher in in vitro-polarized T_H17 cells than in non-polarizing (T_H0) conditions. (viii) T_H1, (ix) T_H2, (x) iT_{reg} (GSE14308)[43], and (xi) T_{FH} signatures (GSE21379)[44], are available at MSigDB (https://www.gsea-msigdb.org/gsea/msigdb/index.jsp).

TR-FRET co-regulator recruitment assay

The DNA sequences that encode the mouse (m)CAR LBD (residues 109–358) were amplified by PCR reaction and inserted into modified pET24b vectors to produce pET24b-mCAR-LBD with an N-terminal 6×His tag. pACYC-Duet1-RXR-LBD, an expression plasmid for the untagged human (h)RXRα LBD, was provided by Dr. Eric Xu[45]. Purification of the mCAR–hRXRα LBD heterodimer, as well as the hRXRα homodimer, was achieved by nickel-affinity chromatography, followed by size-exclusion chromatography in an Akta explorer FPLC (GE Healthcare). In brief, pET24b-mCAR-LBD and pACYC-Duet1-RXR-LBD were co-transformed into BL21 (DE3) cells for the mCAR–hRXRα heterodimer and pET46-RXRα-LBD was transformed into BL21 (DE3) cells for the RXRα homodimer. The cells were grown in 4 × 900 ml of LB medium at 37 °C until the OD_{600} reached 0.6–0.7. Overexpression was induced by 0.3 mM of IPTG and the cells were grown for a further 22 h at 18 °C. The harvested cells were resuspended in sonication buffer (500 mM NaCl, 10 mM HEPES, 10 mM imidazole, pH 8.0, and 10% glycerol), sonicated on an ice-water bath for 20 min at 18 W output, and centrifuged for 25 min at 50,000*g*. The proteins were isolated from the sonicated supernatant by application to a 2-ml His Select column and eluted with a linear gradient from 10 mM to 300 mM imidazole in sonication buffer. The elution fractions containing the proteins concentrated while exchanging buffer to gel filtration buffer (300 mM NaCl, 20 mM HEPES, 1 mM DTT, 5% glycerol). The proteins were purified further by gel filtration through a Superdex 200 26/60 column (GE Healthcare) equilibrated with gel filtration buffer. Fractions containing the proteins were pooled and concentrated to ~8 mg/ml each with 30-kDa cutoff ultrafiltration units (Millipore). TR-FRET assays were performed in low-volume black 384-well plates (Greiner) using 23 μl final well volume. Each well contained the following components in TR-FRET buffer (20 mM KH_2PO_4/K_2HPO_4, pH 8, 50 mM KCl, 5 mM TCEP, 0.005% Tween 20): 4 nM 6×His-CAR–RXRα LBD heterodimer or 6×His-RXRα–RXRα homodimer LBD, 1 nM LanthaScreen Elite Tb-anti-His antibody (ThermoFisher #PV5895), and 400 nM FITC-

labelled PGC1α peptide (residues 137–155, EAEEPSLLKKLLLAPANTQ, containing an N-terminal FITC label with a six-carbon linker, synthesized by Lifetein). Pure ligand (TC, 9-*cis* RA) or tissue extracts (see above) were prepared via serial dilution in vehicle (DMSO or PBS, respectively), and added to the wells along with vehicle control. Plates were incubated at 25 °C for 1 h and fluorescence was measured using a Synergy Neo multi-mode plate reader (BioTek). The terbium (Tb) donor was excited at 340 nm, its emission was monitored at 495 nm, and emission of the FITC acceptor was monitored at 520 nm. Data were plotted as 520/495 nM ratios using Prism software (GraphPad); TC and 9-*cis* RA data were fit to a sigmoidal dose response curve equation.

Statistical analyses

Statistical analyses were performed using Prism (GraphPad). *P* values were determined by paired or unpaired Student's *t*-tests, log-rank test, one-way ANOVA, and two-way ANOVA analyses as appropriate and as listed in the figure legends. The statistical significances of differences (* $P < 0.05$, ** $P < 0.01$, *** $P < 0.001$, **** $P < 0.0001$) are specified throughout the figures and legends. Unless otherwise noted in legends, data are shown as mean ± s.e.m.

Extended Data

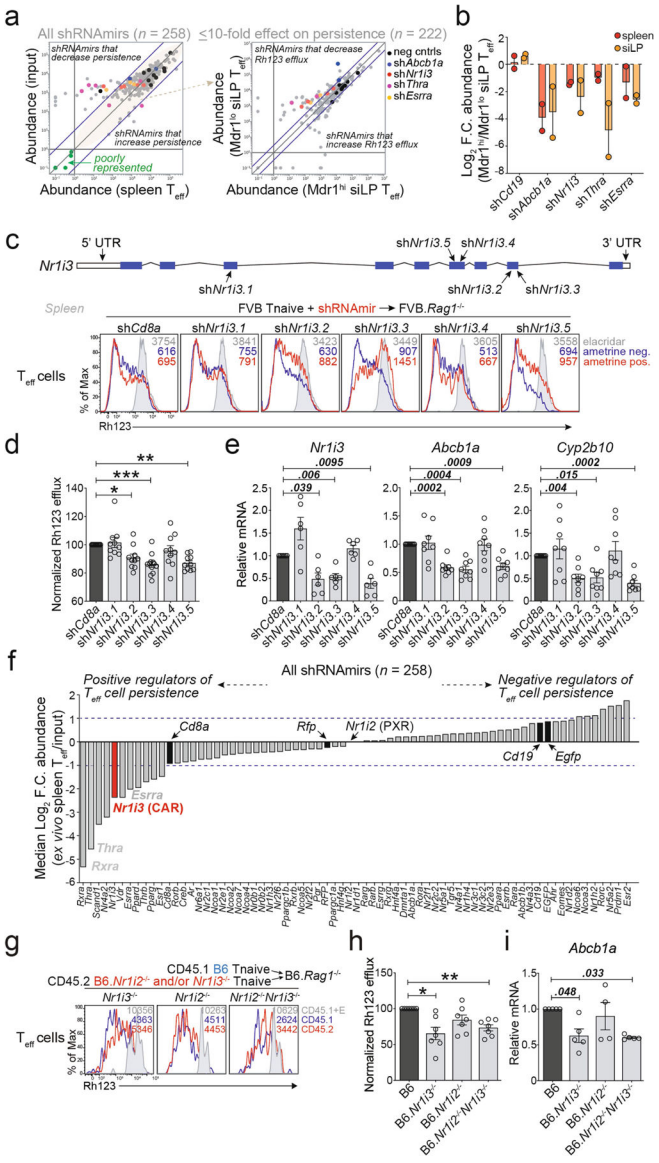

Extended Data Fig. 1 |. Nuclear receptor-dependent regulation of effector T cell persistence and MDR1 expression in vivo.

a, Left, abundance of shRNAmirs in ex vivo-isolated spleen and in vitro-transduced (input) T_{eff} cells. shRNAmirs with one normalized read or fewer in both ex vivo spleen and input T_{eff} cell pools were considered 'poorly represented' (highlighted green). Well-represented shRNAmirs with ≤10-fold change between ex vivo spleen and input T_{eff} cell pools (between blue lines) were considered for downstream analysis. Right, abundance of shRNAmirs, filtered for minimal effects on in vivo T_{eff} cell persistence, in ex vivo-isolated MDR1^{hi} (Rh123^{lo}) and MDR1^{lo} (Rh123^{hi}) siLP T_{eff} cells. **b**, Mean ± s.e.m. $\log_2$[fold change in abundance] of shRNAmirs against *Cd19* (n = 3), *Abcb1a* (n = 2), *Nr1i3* (n = 5), *Thra* (n = 6) and *Esrra* (n = 3) in FVB/N wild-type Rh123^{lo} (MDR1^{hi}) versus Rh123^{hi} (MDR1^{lo}) T_{eff} cells (sorted as in Fig. 1a) recovered from spleens or siLP of transferred FVB/N.*Rag1*$^{-/-}$

mice. **a**, **b**, Data incorporate shRNAmir abundance, determined by DNA-seq, in two independent screens using pooled spleens and siLP from 10 transferred FVB/N.*Rag1*$^{-/-}$ mice per screen. **c**, Top, schematic of the mouse *Nr1i3* locus. Positions of seed sequences for *Nr1i3*-specific shRNAmirs are shown. Untranslated regions (UTRs) are indicated by open boxes. Bottom, ex vivo Rh123 efflux, determined by flow cytometry, in FVB/N wild-type T_{eff} cells transduced with ametrine-expressing retroviruses containing control (sh*CD8a*) or one of five *Nr1i3*-specific shRNAmirs re-isolated from spleens of FVB/N.*Rag1*$^{-/-}$ mice six weeks after T cell transfer. Rh123 efflux in transduced (ametrine^{+}; red) cells is overlaid with that in bystander untransduced (ametrine^{-}; blue) T_{eff} cells from the same mouse. Background Rh123 efflux in untransduced T_{eff} cells treated with the MDR1 inhibitor elacridar is shown in grey. Representative of at least ten mice per group analysed in three independent experiments. **d**, Mean ± s.e.m. normalized ex vivo Rh123 efflux in FVB/N wild-type spleen T_{eff} cells expressing control (sh*Cd8a*; $n = 11$) or *Nr1i3*-specific shRNAmirs (sh*Nr1i3*.1 ($n = 10$), sh*Nr1i3*.2 ($n = 10$), sh*Nr1i3*.3 ($n = 12$), sh*Nr1i3*.4 ($n = 10$) and sh*Nr1i3*.5 ($n = 10$)), determined by flow cytometry as in **c**. Rh123 efflux was normalized to control *shCd8a*-expressing T_{eff} cells after calculating the change (Δ) in Rh123 mean fluorescence intensity (MFI) between bystander transduced (ametrine^{+}) and untransduced (ametrine^{-}) T_{eff} cells. *$P = 0.049$, **$P = 0.003$, ***$P = 0.0006$, one-way ANOVA with Dunnett's correction for multiple comparisons. **e**, Mean ± s.e.m. relative *Abcb1a*, *Nr1i3*, and *Cyp2b10* expression determined by qPCR in FVB/N spleen T_{eff} cells FACS-sorted from FVB/N.*Rag1*$^{-/-}$ recipient mice expressing either a negative control shRNAmir against CD8 (sh*Cd8a*; $n = 8$), or the indicated shRNAmirs against CAR (sh*Nr1i3*.1 ($n = 8$), sh*Nr1i3*.2 ($n = 8$), sh*Nr1i3*.3 ($n = 8$), sh*Nr1i3*.4 ($n = 8$) and sh*Nr1i3*.5 ($n = 8$). $P < 0.05$ versus sh*Cd8a*-expressing cells (one-way ANOVA with Tukey's correction for multiple comparisons) are shown. **f**, Median $\log_2$[fold change] in shRNAmir abundance between FVB/N wild-type ex vivo-isolated spleen and in vitro-transduced (input) T_{eff} cells. **a**, **f**, shRNAmir abundance reflects the mean number of normalized reads, by DNA-seq, in the indicated T_{eff} subsets obtained in two independent screens, each using cells transferred into 10 FVB/N.*Rag1*$^{-/-}$ mice. **g**, Ex vivo Rh123 efflux, determined by flow cytometry, in CD45.1 wild-type (B6; blue) or CD45.2 (red) CAR-deficient (B6.*Nr1i3*$^{-/-}$), PXR-deficient (B6.*Nr1i2*$^{-/-}$) or CAR/PXR double-deficient (B6.*Nr1i3*$^{-/-}$*Nr1i2*$^{-/-}$) T_{eff} cells (gated as in Extended Data Fig. 6a) recovered from spleens of B6.*Rag1*$^{-/-}$ mice six weeks after co-transfer of mixed naive T cells. Background Rh123 efflux in CD45.1 B6 T_{eff} cells treated with the MDR1 inhibitor elacridar is shown in grey. Representative of a total of seven mice per group analysed in two independent experiments. **h**, Mean ± s.e.m. normalized Rh123 efflux in congenically transferred CD45.1 wild-type (B6; $n = 7$) or CD45.2 CAR-deficient (B6.*Nr1i3*$^{-/-}$; $n = 7$), PXR-deficient (B6.*Nr1i2*$^{-/-}$; $n = 7$) or CAR/PXR double-deficient (B6.*Nr1i3*$^{-/-}$*Nr1i2*$^{-/-}$; $n = 7$) spleen T_{eff} cells, determined by flow cytometry as in **g**. *$P < 0.019$, **$P < 0.002$, one-way ANOVA with Tukey's correction for multiple comparisons. **i**, Mean ± s.e.m. relative *Abcb1a* expression determined by ex vivo qPCR in CD45.1 wild-type (B6; $n = 5$) or CD45.2 CAR-deficient (B6.*Nr1i3*$^{-/-}$; $n = 5$), PXR-deficient (B6.*Nr1i2*$^{-/-}$; $n = 4$) or CAR/PXR double-deficient (B6.*Nr1i3*$^{-/-}$*Nr1i2*$^{-/-}$; $n = 5$) spleen T_{eff} cells as in **g**. $P < 0.05$ versus wild-type (B6) T_{eff} cells (one-way ANOVA with Tukey's correction for multiple comparisons) are shown.

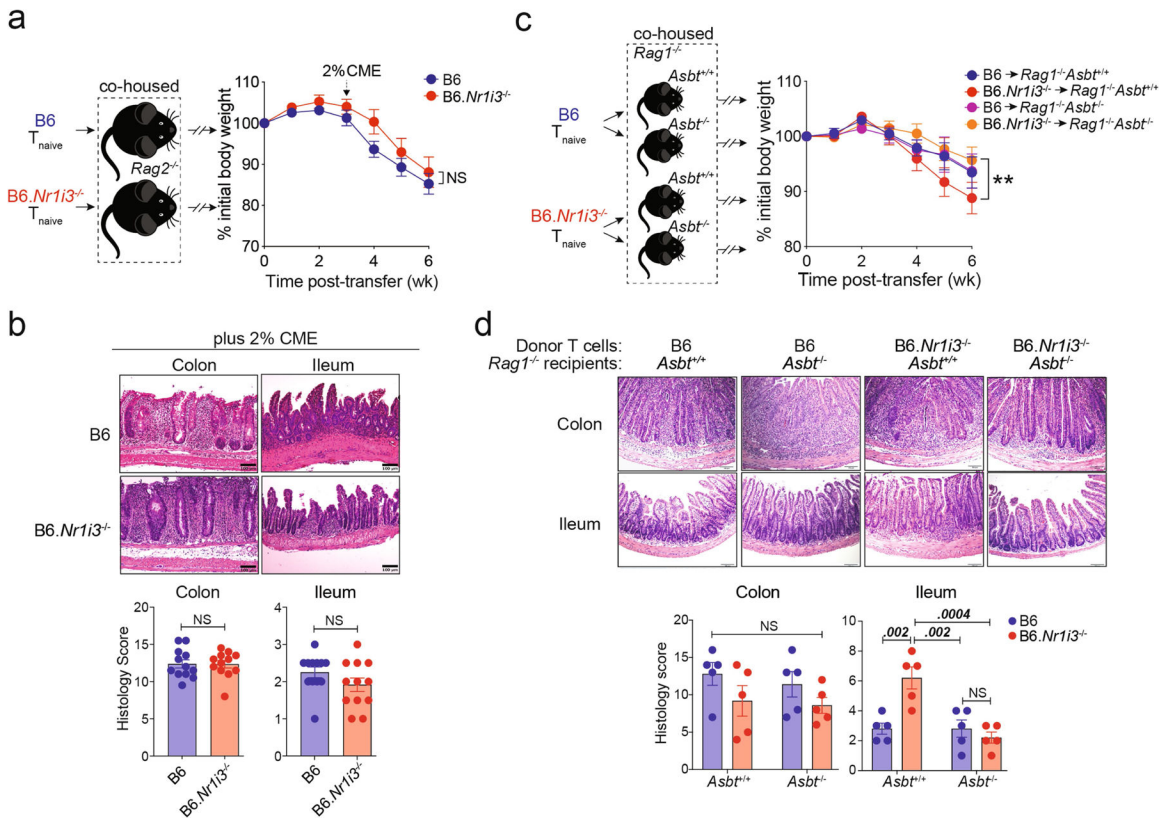

Extended Data Fig. 2 |. Inhibition of bile acid reabsorption rescues ileitis induced by CAR-deficient T cells in reconstituted *Rag*$^{-/-}$ mice.

a, Mean ± s.e.m. weight loss of co-housed B6.*Rag2*$^{-/-}$ mice transplanted with wild-type (B6; blue; $n = 15$) or CAR-deficient (B6.*Nr1i3*$^{-/-}$; red; $n = 13$) naive CD4^{+} T cells and treated with 2% (w:w) cholestyramine (CME) beginning three weeks after T cell transfer. NS, not significant by two-way ANOVA. **b**, Top, H&E-stained sections of colons or terminal ilea from B6.*Rag2*$^{-/-}$ mice reconstituted with wild-type or CAR-deficient T cells and treated with or without CME as in **a**. Representative of 12 mice per group analysed in 3 independent experiments. Magnification, 10×; scale bars, 100 μm. Bottom, mean ± s.e.m. histology scores ($n = 12$) for colons or terminal ilea as in **a**. NS, not significant by unpaired two-tailed Student's *t*-test. **c**, Mean ± s.e.m. weight loss ($n = 16$ per group) of co-housed B6.*Rag1*$^{-/-}$ mice with or without ASBT (encoded by *Slc10a2*) after reconstitution with wild-type (B6) or CAR-deficient (B6.*Nr1i3*$^{-/-}$) naive CD4^{+} T cells. $^{**}P = 0.005$ (CAR-deficient T cell transfer into control versus *Slc10a2*$^{-/-}$*Rag1*$^{-/-}$ recipients), two-way ANOVA. **d**, Top, H&E-stained colon or terminal ileum sections from control or ASBT-deficient B6.*Rag1*$^{-/-}$ mice reconstituted with wild-type or CAR-deficient T cells as in **c**. Representative of five mice per group. Bottom, mean ± s.e.m. histology scores for colons or terminal ilea ($n = 5$) as above. *P* values (one-way ANOVA with Tukey's correction for multiple comparisons) are listed. NS, not significant.

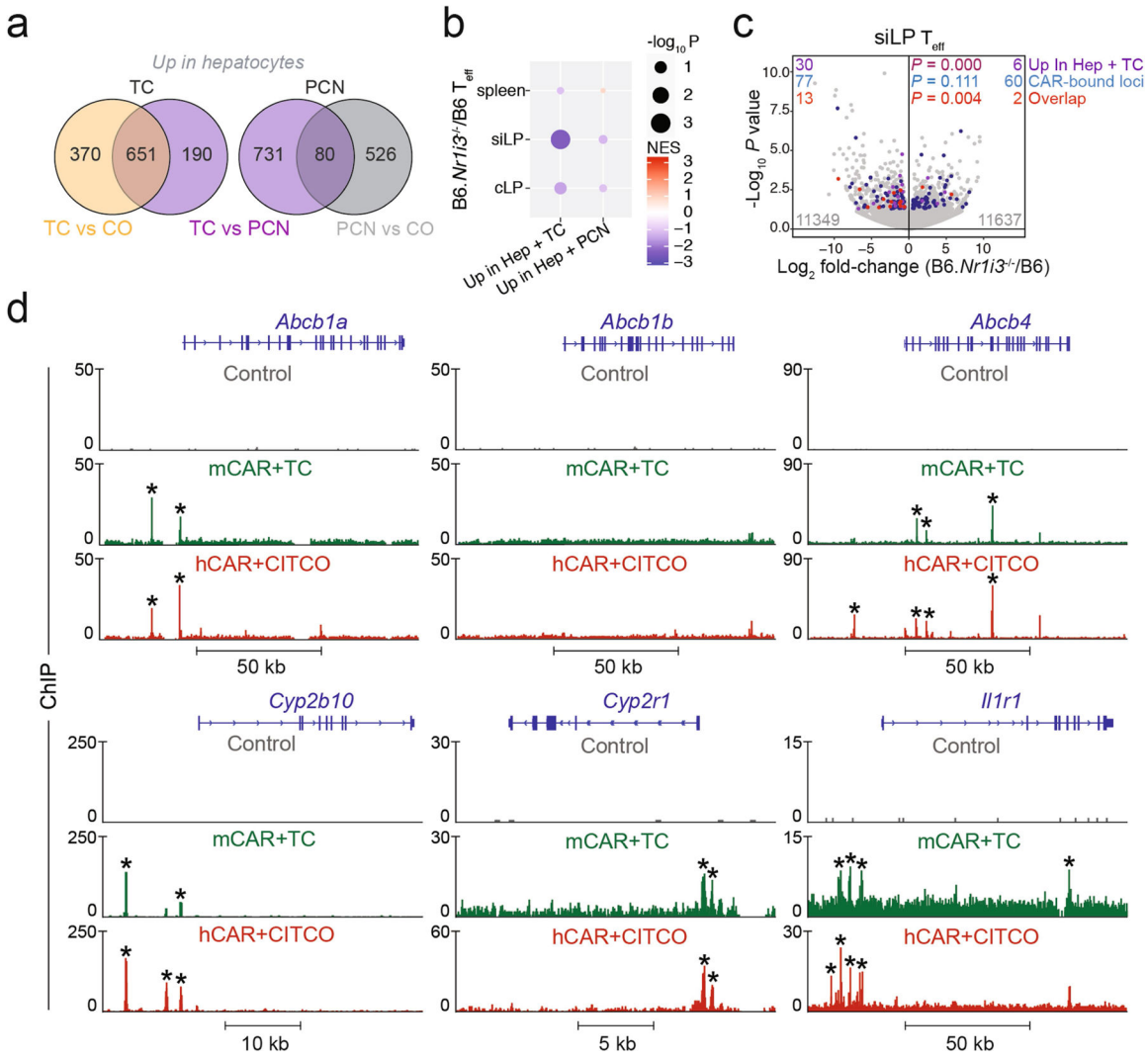

Extended Data Fig. 3 |. Shared features of CAR-dependent gene expression in mucosal T cells and hepatocytes.

a, Overlap between genes induced in B6 wild-type mouse hepatocytes by in vivo treatment with TC or PCN, relative to vehicle (CO, corn oil). **b**, Enrichment of genes induced by TC, but not PCN, in mouse hepatocytes (as in **a**), within those reduced in CAR-deficient (B6.*Nr1i3*$^{-/-}$) versus wild-type (B6) siLP T_{eff} cells from week-3 congenically co-transferred *Rag1*$^{-/-}$ mice (as in Fig. 2a–c). Nominal *P* values compare observed NESs to the null distribution for 1,000 permutations. **c**, Differential gene expression, determined by DESeq2 and shown as a volcano plot, between CAR-deficient (B6.*Nr1i3*$^{-/-}$) and wild-type (B6) siLP T_{eff} cells re-isolated from transferred B6.*Rag1*$^{-/-}$ mice, as in Fig. 2a. Genes induced by TC, but not PCN, treatment in mouse hepatocytes (as in **a**; purple), bound by CAR in ChIP–seq analysis of hepatocytes from TC-treated mice (blue), or both (red) are highlighted. Chi-square *P* values are indicated. **d**, CAR occupancy, determined by ChIP–seq, at representative loci whose expression is regulated by CAR in both mucosal T cells and hepatocytes within mouse hepatocytes ectopically expressing epitope-tagged mouse (m) or human (h) CAR

proteins and re-isolated from mice after treatment with TC or CITCO. *False discovery rate (FDR) $q < 0.05$ determined using MACS2 base settings.

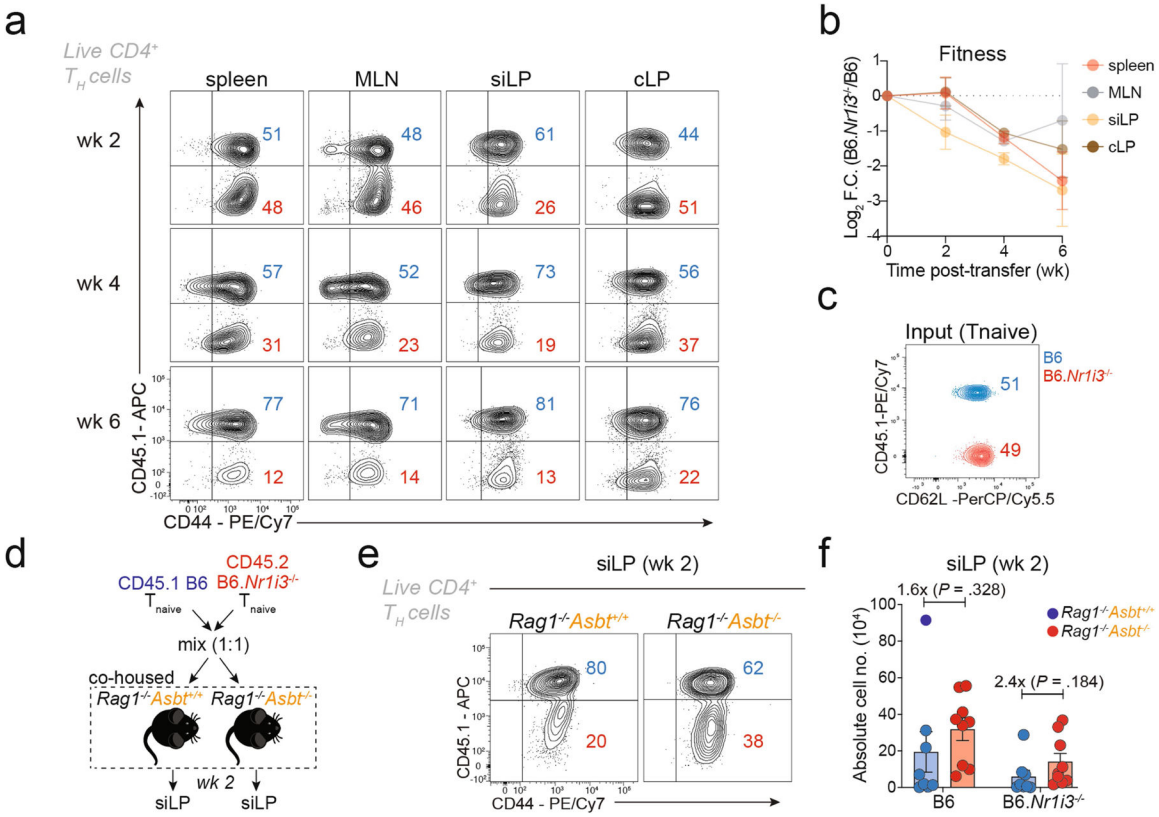

Extended Data Fig. 4 |. CAR promotes effector T cell persistence in the presence of small intestinal bile acids.

a, Percentages of live CD44^{hi} wild-type (B6; CD45.1^{+}; blue) or CAR-deficient (B6.*Nr1i3*$^{-/-}$; CD45.1^{-}; red) T_{eff} cells, determined by flow cytometry and gated as in Extended Data Fig. 6a, in tissues from reconstituted B6.*Rag1*$^{-/-}$ mice over time. Numbers indicate percentages; representative of five mice per tissue and time point. **b**, Fitness, defined as mean ± s.e.m. $\log_2$[fold change (F.C.)] of CAR-deficient (B6.*Nr1i3*$^{-/-}$) versus wild-type (B6) T_{eff} cell percentages ($n = 5$) in tissues from congenically co-transferred *Rag1*$^{-/-}$ mice over time, determined by flow cytometry as in **a**. **c**, Percentage of wild-type (B6, CD45.1^{+}; blue) and CAR-deficient (B6.*Nr1i3*$^{-/-}$, CD45.1^{-}; red) naive (CD62L^{hi}) CD4^{+} T cells after sorting and mixing, and before in vivo transfer into *Rag1*$^{-/-}$ mice (input T_{naive}); representative of three mixtures used for analysing resulting T_{eff} cells at 2, 4 or 6 weeks after transfer. **d**, Equal numbers of CD45.1 wild-type (B6; blue) and CD45.2 CAR-deficient (B6.*Nr1i3*$^{-/-}$; red) naive CD4^{+} T cells were transferred together into co-housed *Rag1*$^{-/-}$ mice with or without the ileal bile acid reuptake transporter ASBT (gene symbol *Slc10a2*). The resulting T_{eff} cells from siLP were analysed two weeks after T cell transfer via flow cytometry. **e**, Percentages of live CD44^{hi} wild-type (B6; CD45.1^{+}; blue) or CAR-deficient (B6.*Nr1i3*$^{-/-}$; CD45.1^{-}; red) T_{eff} cells, determined by flow cytometry and gated as in Extended Data Fig. 6a, in siLP from week-2 reconstituted B6.*Rag1*$^{-/-}$ mice. Numbers indicate percentages; representative of 8–10 mice analysed over two independent

experiments. **f**, Mean ± s.e.m. absolute numbers of live CD45.1 wild-type (B6; left) or CD45.2 CAR-deficient (B6.*Nr1i3*$^{-/-}$; right) T_{eff} cells, determined by ex vivo flow cytometry as in **e**, from siLP two weeks after mixed T cell transfer into control (*Slc10a2*$^{+/+}$; blue; $n = 8$) or ASBT-deficient (*Slc10a2*$^{-/-}$; red; $n = 10$) *Rag1*$^{-/-}$ recipients. Fold changes in cell numbers recovered from ASBT-deficient versus control recipients, as well as *P* values (two-tailed unpaired Student's *t*-test), are indicated.

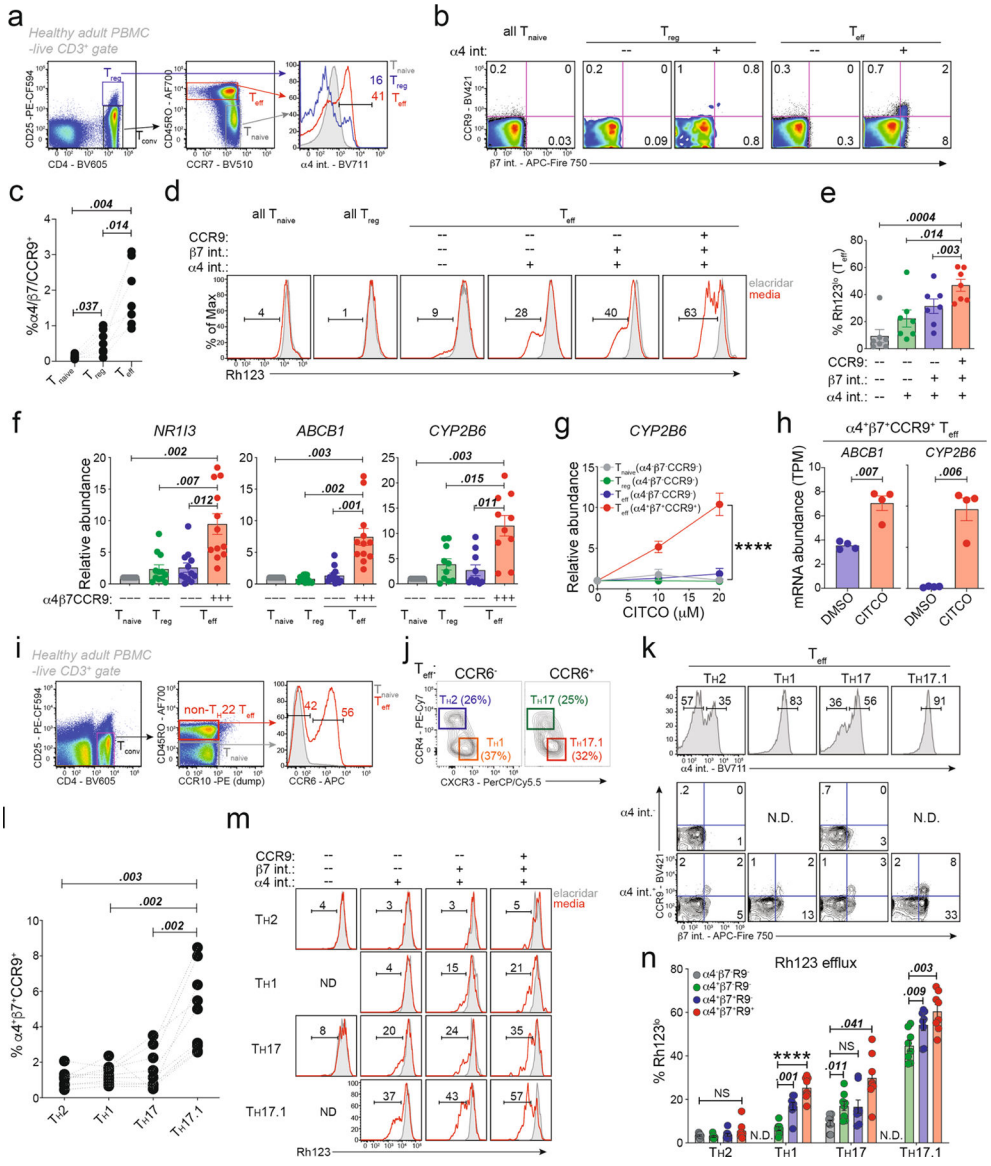

Extended Data Fig. 5 |. Preferential CAR expression and function in human T_{eff} cells expressing small bowel homing receptors.

a, FACS-based identification of human CD4$^+$ T cell subsets in PBMCs from healthy adult human donors. Right, expression of integrin α4 (α4 int.) in gated naive (grey), T_{reg} (blue), and T_{eff} (red) T cells. **b**, Expression of integrin β7 (β7 int.) and CCR9 in total naive CD4$^+$ T cells, or in α4 int. with or without T_{reg} or T_{eff} subsets (gated as in **a**). Representative of seven independent experiments using PBMCs from different donors. **c**, Percentages

of $\alpha4^+\beta7^+CCR9^+$ naive T, T_{reg}, and T_{eff} cells, determined by flow cytometry as in **a**, **b**. Individual data points for seven independent experiments are shown and connected by lines. *P* values (one-way ANOVA with Tukey's correction for multiple comparisons) are shown. **d**, Ex vivo Rh123 efflux in $CD4^+$ T cell subsets (gated as in **a**, **b**) in the presence (grey) or absence (red) of the selective MDR1 inhibitor elacridar. Representative of seven experiments. **e**, Mean ± s.e.m. percentages ($n = 7$) of $Rh123^{lo}$ ($MDR1^+$) T_{eff} subsets, determined by flow cytometry as in **d**. *P* values (one-way ANOVA with Tukey's correction for multiple comparisons) are shown. **f**, Mean ± s.e.m. ex vivo expression, determined by qPCR, of *NR1I3* ($n = 12$), *ABCB1* ($n = 12$) and *CYP2B6* ($n = 10$) in $\alpha4^-\beta7^-CCR9^-$ and $\alpha4^+\beta7^+CCR9^+$ naive T, T_{reg} and T_{eff} cells, FACS-sorted as in **a**, **b**. *P* values (one-way ANOVA with Tukey's correction for multiple comparisons) are shown. **g**, Mean ± s.e.m. relative *CYP2B6* expression ($n = 5$), determined by qPCR, in $CD4^+$ T cell subsets (as in **f**) stimulated ex vivo in the presence of titrating concentrations of CITCO. Gene expression analysed 24 h after activation. ***$P < 0.0001$ by two-way ANOVA. **h**, Mean ± s.e.m. normalized *ABCB1* or *CYP2B6* expression, determined by RNA-seq and presented as TPM, in FACS-sorted $\alpha4^+\beta7^+CCR9^+$ T_{eff} cells stimulated in vitro with or without CITCO. Data from four independent RNA-seq experiments using cells sorted from different healthy adult donors; *P* values (paired two-tailed Student's *t*-test) are indicated. **i**, Identification of $CD4^+$ naive (T_{naive}; $CD25^-CD45RO^-$; grey) or T_{eff} ($CD25^-CD45RO^+$; red) cells, by flow cytometry, from healthy adult human PBMCs. For improved purity of T_H1, T_H2, T_H17 and $T_H17.1$ cells, CCR10-expressing T_H22 cells were excluded. CCR6 expression in naive T (grey) or non-T_H22 T_{eff} cells (red) is shown on the right; $CCR6^+$ or $CCR6^-$ T_{eff} cells were gated to enrich for T_H17 or non-T_H17 lineages, respectively. **j**, Expression of CCR4 and CXCR3 in $CCR6^-$ (non-T_H17; left) or $CCR6^+$ (T_H17; right) T_{eff} cells identifies enriched $CCR6^-CCR4^{lo}CXCR3^{hi}$ (T_H1; orange), $CCR6^-CCR4^{hi}CXCR3^{lo}$ (T_H2; blue), $CCR6^+CCR4^{hi}CXCR3^{lo}$ (T_H17; green), and $CCR6^+CCR4^{lo}CXCR3^{hi}$ ($T_H17.1$; red) subsets. **k**, Expression of integrin α4 (α4 int.; top) in T_H2, T_H1, T_H17 and $T_H17.1$ human T_{eff} cells gated as in **a**, **b**. Expression of integrin β7 (β7 int.) and CCR9 within $\alpha4\ int^-$ (middle) or $\alpha4\ int^+$ (bottom) T_H2, T_H1, T_H17 or $T_H17.1$ cells gated as above. **i**–**k**, Representative of nine independent experiments using PBMCs from different healthy adult donors. **l**, Percentages ($n = 9$) of $\alpha4^+\beta7^+CCR9^+$ cells (gated as in **a**, **b**) amongst ex vivo T_H1, T_H2, T_H17 and $T_H17.11$ T_{eff} cells (gated as in **i**–**k**). Data from independent donors are connected by lines; *P* values (one-way ANOVA with Tukey's correction for multiple comparisons) are shown. **m**, MDR1-dependent Rh123 efflux in the indicated T_H1, T_H2, T_H17 and $T_H17.1$ T_{eff} subsets gated by expression of α4 int., β7 int., and/or CCR9 in the presence (grey) or absence (red) of elacridar. Representative of eight independent experiments using PBMCs from different donors. **n**, Mean ± s.e.m. percentages ($n = 8$) of $Rh123^{lo}$ ($MDR1^+$) cells within T_H1, T_H2, T_H17 and $T_H17.11$ T_{eff} subsets gated according to expression of α4 int., β7 int., and/or CCR9 as in **e**. *P* values (one-way ANOVA with Tukey's correction for multiple comparisons) are indicated; ****$P < 0.0001$. N.D., not detected; NS, not significant.

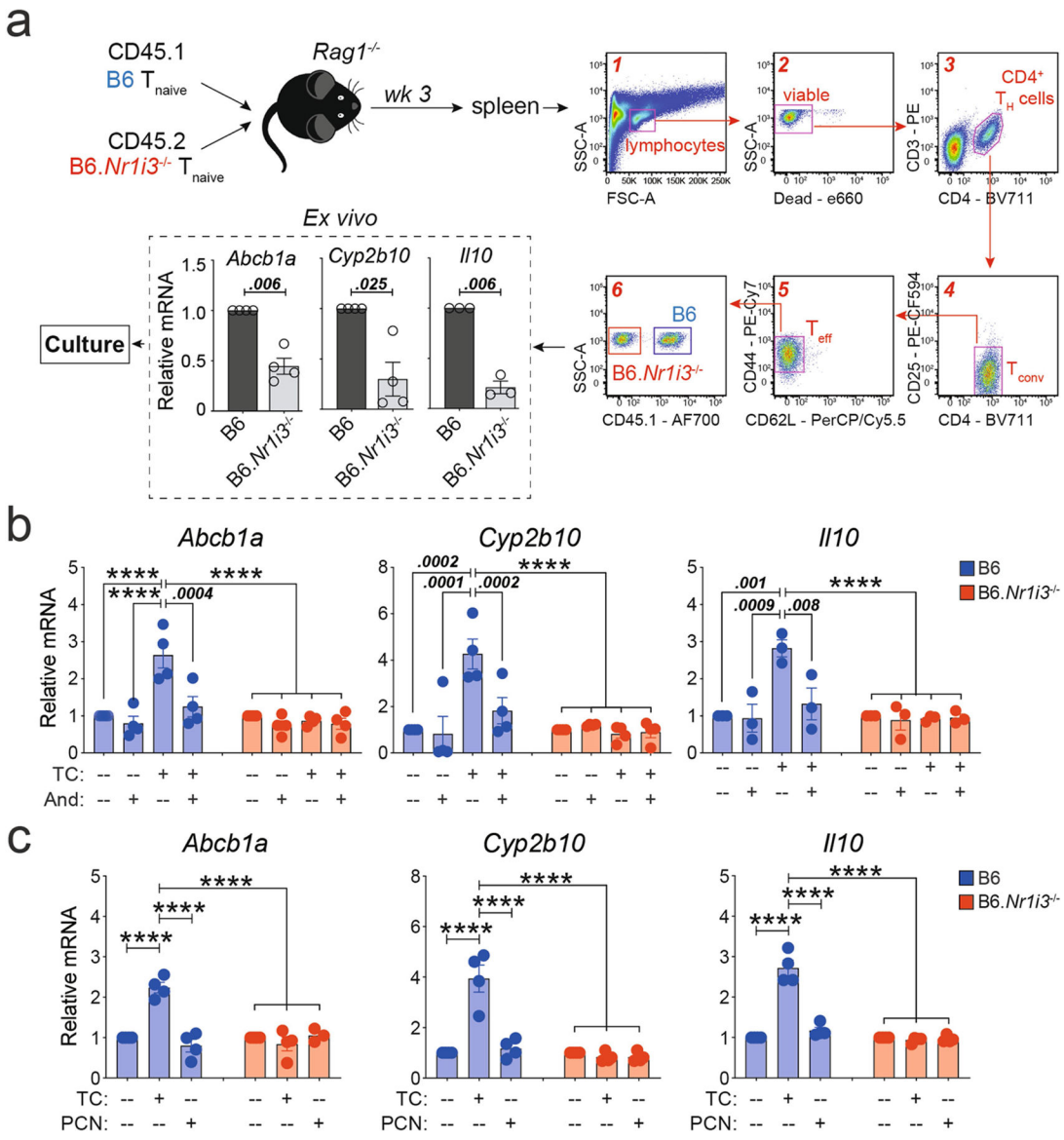

Extended Data Fig. 6 |. TCPOBOP promotes CAR-dependent gene expression in ex vivo-isolated effector T cells.

a, Top left, equal numbers of CD45.1 wild-type (B6; blue) and CD45.2 CAR-deficient (B6.*Nr1i3*$^{-/-}$; red) naive CD4^{+} T cells were transferred together into B6.*Rag1*$^{-/-}$ mice. The resulting T_{eff} cells were FACS-purified from spleen after 3 weeks. Right, sequential gating strategy for re-isolating wild-type and CD45.2 CAR-deficient spleen T_{eff} cells. Bottom left, mean ± s.e.m. relative expression of *Abcb1a* ($n = 4$), *Cyp2b10* ($n = 4$), and *Il10* ($n = 3$), determined by qPCR, in ex vivo-isolated wild-type (B6) or CAR-deficient (B6.*Nr1i3*$^{-/-}$) spleen T_{eff} cells. These cells were used for ex vivo stimulation experiments with or without small-molecule ligands (**b**, **c**). *P* values (paired two-tailed Student's *t*-test) are indicated. **b**, Mean ± s.e.m. relative expression of *Abcb1a* ($n = 4$), *Cyp2b10* ($n = 4$), and *Il10* ($n = 3$), by qPCR, in wild-type (B6) or CAR-deficient T_{eff} cells isolated from transferred *Rag1*$^{-/-}$ mice (as in **a**), and stimulated ex vivo with anti-CD3 and anti-CD28 antibodies in the presence or absence of TC (10 μM), the mCAR inverse agonist And (10 μM), or both. *P* values

(one-way ANOVA with Tukey's correction for multiple comparisons) are indicated; ****P < 0.0001. **c**, Mean ± s.e.m. relative expression of *Abcb1a*, *Cyp2b10*, and *Il10* (n = 5), determined by qPCR, in wild-type (B6) or CAR-deficient (B6.*Nr1i3*$^{-/-}$) T_{eff} cells isolated and stimulated as in **a**, **b** in the presence or absence of TC (10 μM) or PCN (10 μM). Data are presented as fold change in mRNA abundance relative to vehicle-treated cells (DMSO for TC; ethanol for PCN). ****P < 0.0001, one-way ANOVA with Dunnett's correction for multiple comparisons. NS, not significant.

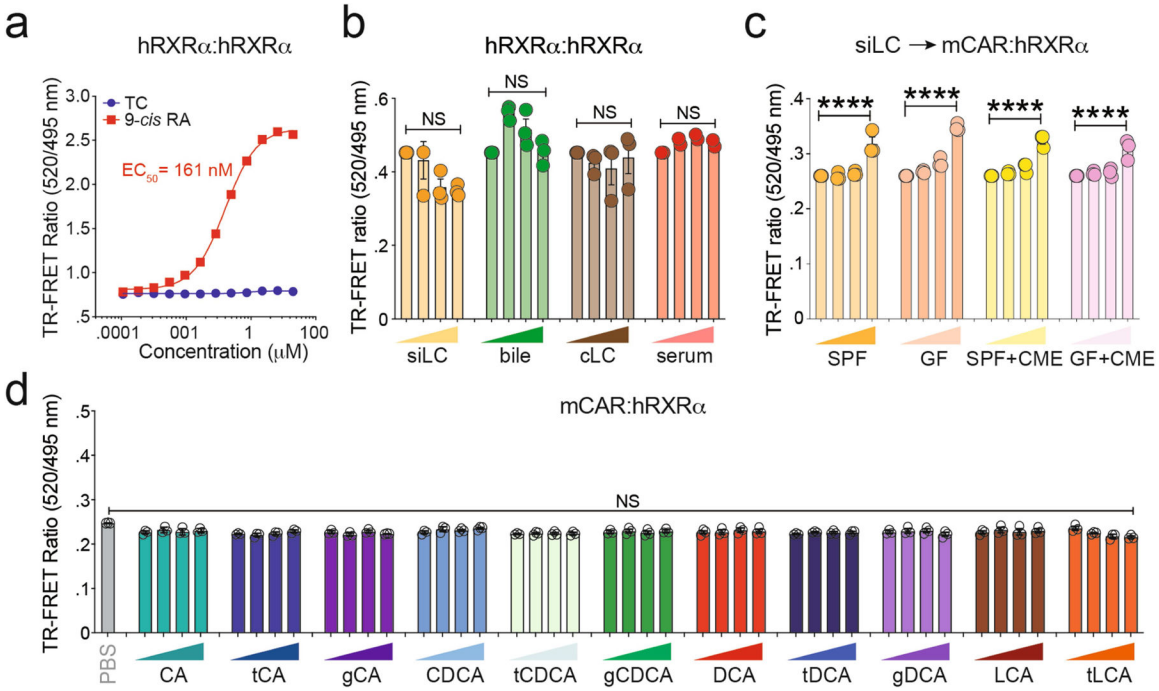

Extended Data Fig. 7 |. Characteristics of endogenous intestinal metabolites that activate the CAR LBD.

a, Mean ± s.e.m. activation (triplicate samples) of recombinant hRXRα LBD homodimers, determined by TR-FRET in the presence of TC (blue) or 9-*cis* retinoic acid (RA; red). Median effective concentration (EC_{50}) of 9-*cis* RA-dependent hRXRα LBD homodimer activation is indicated. Representative of more than five independent experiments. **b**, Mean ± s.e.m. activation (n = 3) of hRXRα LBD homodimers, determined by TR-FRET as in **a**, in the presence of titrating concentrations of siLC, bile, cLC or serum from wild-type B6 mice. NS, not significant by one-way ANOVA with Dunnett's correction for multiple comparisons. **c**, Mean ± s.e.m. activation (n = 3) of CAR–RXR LBD heterodimers, determined by TR-FRET, in the presence of titrating concentrations of siLC isolated from wild-type B6 mice housed under specific pathogen-free (SPF) or germ-free (GF) conditions and pre-treated with or without cholestyramine (CME) to deplete free bile acids. ****P < 0.0001, one-way ANOVA with Dunnett's correction for multiple comparisons. **a**–**c**, The bars for each tissue extract indicate dilution series (left to right): diluent (PBS) alone; 0.01%, 0.1%, 1%. Data are shown from three independent experiments using extracts from different wild-type mice, with each concentration from each individual mouse run in triplicate. **d**, Mean ± s.e.m. TR-FRET signals (n = 3) of CAR–RXR LBD heterodimers in the presence of

titrating concentrations of individual bile acid (BA) species. NS, not significant by one-way ANOVA with Dunnett's correction for multiple comparisons. The bars for bile acids indicate concentrations (left to right): vehicle (DMSO), 10 μM, 100 μM, 1,000 μM. Data are shown from three independent experiments, in which each bile acid concentration was run in triplicate.

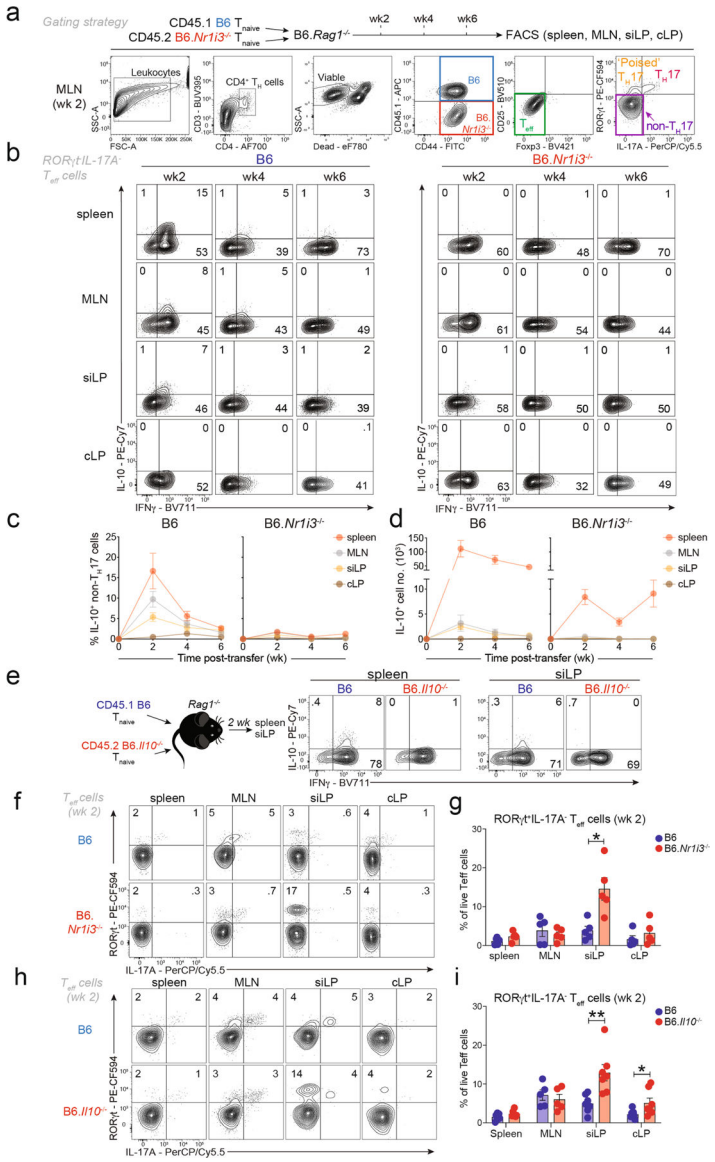

Extended Data Fig. 8 |. CAR promotes IL-10 expression in mucosal T_{eff} cells and regulates T_R1 and T_H17 cell development in the small intestine.

a, Equal numbers of CD45.1 wild-type (B6; blue) and CD45.2 CAR-deficient (B6.*Nr1i3*$^{-/-}$; red) naive CD4$^+$ T cells were transferred together into *Rag1*$^{-/-}$ mice. The resulting T_{eff} cells were analysed using surface and intracellular flow cytometry after ex vivo stimulation with PMA and ionomycin at 2, 4, and 6 weeks from spleen, MLN, siLP, or cLP. Gating hierarchy is shown from a representative sample of MLN mononuclear cells at two weeks after T cell transfer. **b**, Intracellular IL-10 and IFN**γ** expression, determined by flow cytometry, in

wild-type (B6, blue; left) and CAR-deficient (B6.*Nr1i3*$^{-/-}$, red; right) non-T_H17 T_{eff} cells, gated as in **a**, from tissues of T cell-reconstituted B6.*Rag1*$^{-/-}$ mice over time. Numbers indicate percentages; representative of five mice per tissue and time point. **c**, **d**, Mean ± s.e.m. percentages (**c**) or numbers (**d**) ($n = 5$) of IL-10-expressing wild-type (B6, left) or CAR-deficient (B6.*Nr1i3*$^{-/-}$, right) T_{eff} cells, determined by ex vivo flow cytometry as in **a**, **b** from tissues of transferred B6.*Rag1*$^{-/-}$ mice over time. **e**, Specificity of IL-10 intracellular staining, as validated by analysis of IL-10 production by CD45.1 wild-type (B6; blue) or CD45.2 *Il10*$^{-/-}$ (red) T_{eff} cells isolated from spleen or siLP of congenically co-transferred *Rag1*$^{-/-}$ mice. Representative of six mice analysed over two independent experiments. **f**, Expression of RORγt and IL-17A, determined by intracellular FACS analysis as in Extended Data Fig. 8a, in wild-type (B6) or CAR-deficient (B6.*Nr1i3*$^{-/-}$) $CD4^+$ T_{eff} cells from tissues of reconstituted *Rag1*$^{-/-}$ mice two weeks after mixed T cell transfer. Numbers indicate percentages; representative of five mice per tissue and time point. **g**, Mean ± s.e.m. percentages of ($n = 5$) wild-type (B6; blue) or CAR-deficient (B6.*Nr1i3*$^{-/-}$; red) RORγt$^+$IL-17A$^-$ T_{eff} cells, determined by intracellular flow cytometry as in **a**. *$P = 0.029$, paired two-tailed Student's *t*-test. **h**, Expression of RORγt and IL-17A, determined by intracellular FACS analysis, in wild-type (B6) or *Il10*$^{-/-}$ T_{eff} cells from tissues of reconstituted *Rag1*$^{-/-}$ mice two weeks after mixed T cell transfer. Numbers indicate percentages; representative of five mice per tissue and time point. **i**, Mean ± s.e.m. percentages of ($n = 7$) wild-type (B6; blue) or *Il10*$^{-/-}$ (red) RORγt$^+$IL-17A$^-$ T_{eff} cells, determined by intracellular flow cytometry as in **c**. *$P = 0.033$, **$P = 0.0099$, paired two-tailed Student's *t*-test.

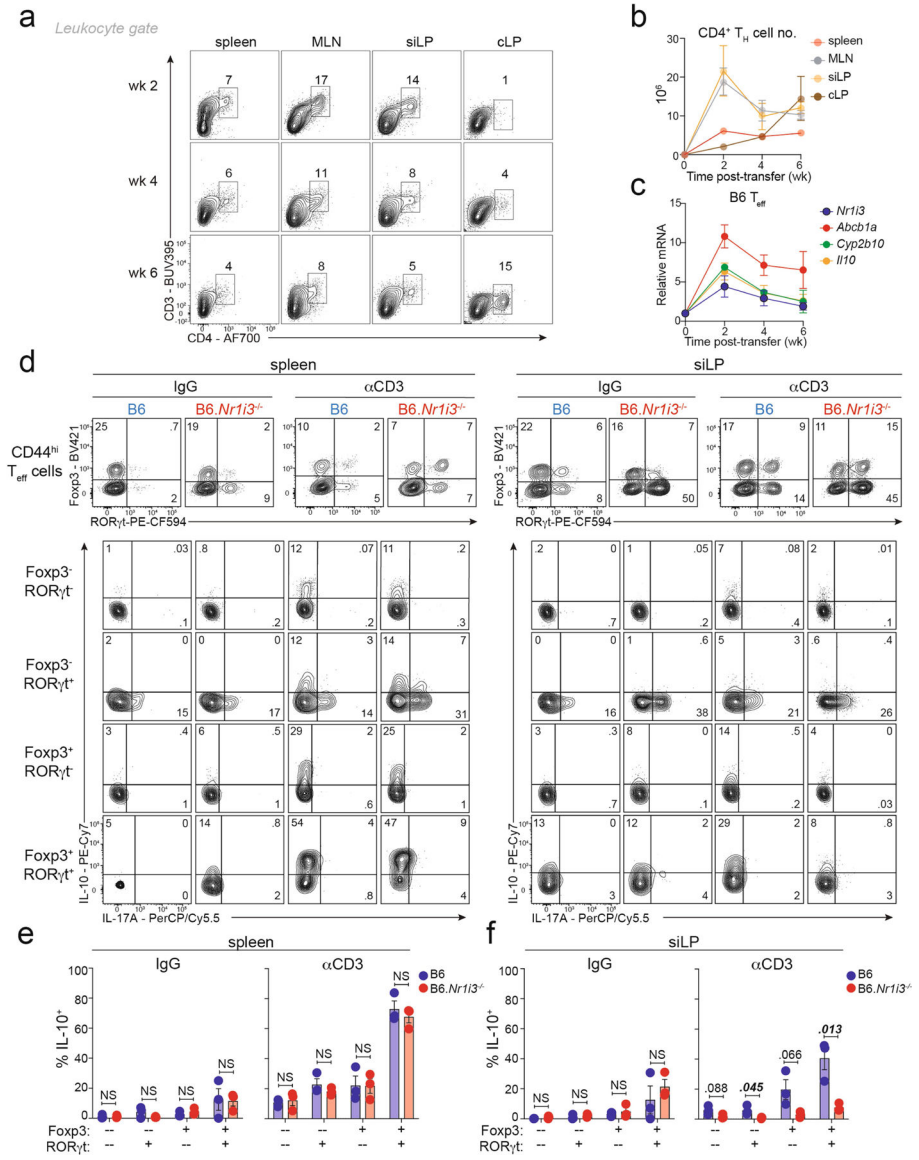

Extended Data Fig. 9 |. CAR expression and function in mucosal T_{eff} cells is increased in response to intestinal inflammation.

a, Percentages of $CD3^+CD4^+$ T cells in tissues from *Rag1*$^{-/-}$ mice transplanted with congenic mixtures of wild-type and CAR-deficient naive $CD4^+$ T cells over time, determined by flow cytometry. Representative of five mice per tissue and time point. **b**, Mean ± s.e.m. absolute numbers of $CD3^+CD4^+$ T_H cells ($n = 5$) in tissues from transferred B6.*Rag1*$^{-/-}$ mice over time, determined by flow cytometry as in **a. c**, Mean ± s.e.m. relative ex vivo *Nr1i3*, *Abcb1a*, *Cyp2b10*, and *Il10* gene expression ($n = 3$), determined by qPCR, in wild-type (B6) $CD4^+$ T_{eff} cells (sorted as in Extended Data Fig. 8a) from spleens of transferred B6.*Rag1*$^{-/-}$ mice over time. **d**, Top, expression of FOXP3 and RORγt, determined by intracellular staining after ex vivo (PMA + ionomycin) stimulation, in $CD4^+CD44^{hi}$ cells from spleen (left) or siLP (right) of wild-type (B6, blue) or CAR-deficient (B6.*Nr1i3*$^{-/-}$, red) mice injected with isotype control (IgG) or soluble anti-CD3. Bottom, expression of IL-10 and IL-17A in wild-type or CAR-deficient spleen

or siLP T cell subsets from mice treated with isotype control (IgG) or anti-CD3 antibodies. Cells were gated and analysed by flow cytometry as above. Numbers indicate percentages; representative of three mice per group and genotype analysed over two independent experiments. **e**, **f**, Mean ± s.e.m. percentages of IL-10-expressing T cell subsets (n = 3), gated and analysed by ex vivo flow cytometry as in **a**, in spleen (**e**) or siLP (**f**) T_H cell subsets from wild-type (B6, blue) or CAR-deficient (B6.*Nr1i3*$^{-/-}$, red) mice injected with isotype control (IgG) or anti-CD3 antibody. P values (unpaired Student's t-test) are indicated; NS, not significant.

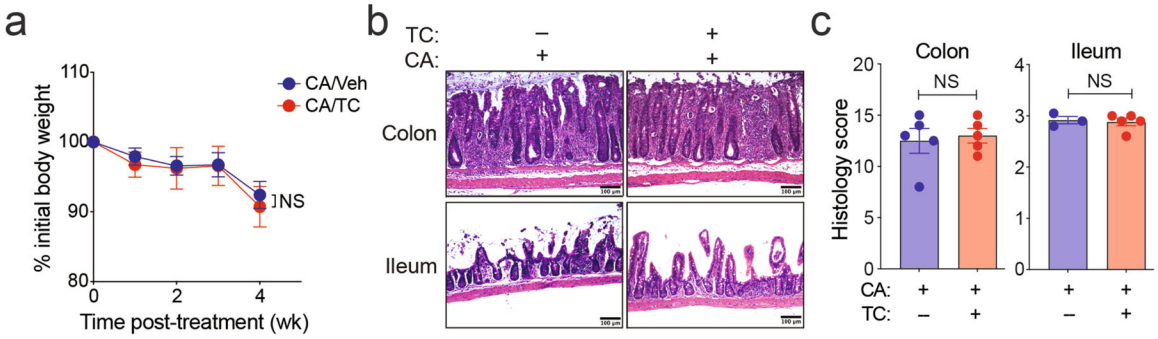

Extended Data Fig. 10 |. TCPOBOP protection against bile acid-induced ileitis requires CAR expression in T cells.

a, Mean ± s.e.m. weight loss (n = 5 per group) of co-housed B6.*Rag2*$^{-/-}$ mice transplanted with CAR-deficient (B6.*Nr1i3*$^{-/-}$) CD4$^+$ naive T cells and maintained on a cholic acid-supplemented diet with (CA/TC) or without (CA/Veh) TC treatment. Weights are shown relative to three weeks after transfer, when TC treatments were initiated. NS, not significant; two-way ANOVA. **b**, H&E-stained sections of terminal ilea or colons from B6.*Rag2*$^{-/-}$ mice reconstituted with CAR-deficient T cells and treated as above and as indicated. Representative of five mice per group analysed in two independent experiments. Magnification, 10×; scale bars, 100 μm. **c**, Mean ± s.e.m. histology scores for colons and terminal ilea as in **a.** NS, not significant by unpaired two-tailed Student's t-test.

Supplementary Material

Refer to Web version on PubMed Central for supplementary material.

Acknowledgements

We thank Core Facility staff at Scripps Florida and Baylor College of Medicine for technical support, and P. Dawson and A. Rao for discussions. This work was supported by Scripps Florida via the State of Florida (M.S.S.), the R. P. Doherty Jr.–Welch Chair in Science Q-0022 at Baylor College of Medicine (D.D.M.), National Institute of Health grants R21AI119728 (M.S.S.), R01AI118931 (M.S.S.), U19AI109976 (M.E.P.), P01AI145815 (M.E.P.), R01DK113789 (C.T.W.) and F30DK127865 (B.F.), and Crohn's and Colitis Foundation (CCF) grants (Senior Research Award no. 422515 (M.S.S.) and Litwin IBD pioneer award no. 572171 (H.W.)).

Data availability

RNA-seq data for mouse (GSE149218) and human (GSE149219) CD4$^+$ T cells described here are publicly available at the NCBI Gene Expression Omnibus (GEO) repository (series no. GSE149220). Sequence and other information related to shRNAmir retroviral constructs

used in the pooled in vivo RNAi screen (related to Fig. 1, Extended Data Fig. 1), as well as complete gene lists derived from differential gene expression analyses of wild-type and *Nr1i3*$^{-/-}$ T_{eff} cells (related to Figs. 2a–d, 3a–c) and statistical analysis of differences between in vitro-polarized wild-type and *Nr1i3*$^{-/-}$ CD4^{+} T cells (related to Fig. 3h, i), are available in the Supplementary Information. Other relevant data are available from the corresponding authors upon reasonable request. Previously generated ChIP–seq and RNA-seq datasets analysed in this study include GEO accession numbers GSE104734, GSE112199, GSE92940 and GSE21670. Datasets obtained from the Molecular Signature Database (MSigDB; https://www.gsea-msigdb.org/) derive from GEO accession numbers GSE14308 and GSE21379. Source data are provided with this paper.

References

1. Hofmann AF & Hagey LR Key discoveries in bile acid chemistry and biology and their clinical applications: history of the last eight decades. J. Lipid Res 55, 1553–1595 (2014). [PubMed: 24838141]
2. Poupon R, Chazouillères O & Poupon RE Chronic cholestatic diseases. J. Hepatol 32 (Suppl. 1), 129–140 (2000). [PubMed: 10728800]
3. Arab JP, Karpen SJ, Dawson PA, Arrese M & Trauner M Bile acids and nonalcoholic fatty liver disease: Molecular insights and therapeutic perspectives. Hepatology 65, 350–362 (2017). [PubMed: 27358174]
4. Cao W et al. The xenobiotic transporter Mdr1 enforces T cell homeostasis in the presence of intestinal bile acids. Immunity 47, 1182–1196 (2017). [PubMed: 29262351]
5. Lazar MA Maturing of the nuclear receptor family. J. Clin. Invest 127, 1123–1125 (2017). [PubMed: 28368290]
6. Chen R et al. In vivo RNA interference screens identify regulators of antiviral CD4^{+} and CD8^{+} T cell differentiation. Immunity 41, 325–338 (2014). [PubMed: 25148027]
7. Ludescher C et al. Detection of activity of P-glycoprotein in human tumour samples using rhodamine 123. Br. J. Haematol 82, 161–168 (1992). [PubMed: 1358171]
8. Zhang J, Huang W, Qatanani M, Evans RM & Moore DD The constitutive androstane receptor and pregnane X receptor function coordinately to prevent bile acid-induced hepatotoxicity. J. Biol. Chem 279, 49517–49522 (2004). [PubMed: 15358766]
9. Cerveny L et al. Valproic acid induces CYP3A4 and MDR1 gene expression by activation of constitutive androstane receptor and pregnane X receptor pathways. Drug Metab. Dispos 35, 1032–1041 (2007). [PubMed: 17392393]
10. Wei P, Zhang J, Egan-Hafley M, Liang S & Moore DD The nuclear receptor CAR mediates specific xenobiotic induction of drug metabolism. Nature 407, 920–923 (2000). [PubMed: 11057673]
11. Evans RM & Mangelsdorf DJ Nuclear receptors, RXR, and the big bang. Cell 157, 255–266 (2014). [PubMed: 24679540]
12. Staudinger JL et al. The nuclear receptor PXR is a lithocholic acid sensor that protects against liver toxicity. Proc. Natl Acad. Sci. USA 98, 3369–3374 (2001). [PubMed: 11248085]
13. Ostanin DV et al. T cell transfer model of chronic colitis: concepts, considerations, and tricks of the trade. Am. J. Physiol. Gastrointest. Liver Physiol 296, G135–G146 (2009). [PubMed: 19033538]
14. Arnold MA et al. Colesevelam and colestipol: novel medication resins in the gastrointestinal tract. Am. J. Surg. Pathol 38, 1530–1537 (2014). [PubMed: 24921636]
15. Dawson PA, Lan T & Rao A Bile acid transporters. J. Lipid Res 50, 2340–2357 (2009). [PubMed: 19498215]
16. Cui JY & Klaassen CD RNA-seq reveals common and unique PXR- and CAR-target gene signatures in the mouse liver transcriptome. Biochim. Biophys. Acta 1859, 1198–1217 (2016). [PubMed: 27113289]

17. Niu B et al. In vivo genome-wide binding interactions of mouse and human constitutive androstane receptors reveal novel gene targets. Nucleic Acids Res 46, 8385–8403 (2018). [PubMed: 30102401]
18. De Calisto J et al. T-cell homing to the gut mucosa: general concepts and methodological considerations. Methods Mol. Biol 757, 411–434 (2012). [PubMed: 21909925]
19. Maglich JM et al. Identification of a novel human constitutive androstane receptor (CAR) agonist and its use in the identification of CAR target genes. J. Biol. Chem 278, 17277–17283 (2003). [PubMed: 12611900]
20. Ramesh R et al. Pro-inflammatory human Th17 cells selectively express P-glycoprotein and are refractory to glucocorticoids. J. Exp. Med 211, 89–104 (2014). [PubMed: 24395888]
21. Moore LB et al. Pregnane X receptor (PXR), constitutive androstane receptor (CAR), and benzoate X receptor (BXR) define three pharmacologically distinct classes of nuclear receptors. Mol. Endocrinol 16, 977–986 (2002). [PubMed: 11981033]
22. Karwacz K et al. Critical role of IRF1 and BATF in forming chromatin landscape during type 1 regulatory cell differentiation. Nat. Immunol 18, 412–421 (2017). [PubMed: 28166218]
23. Gagliani N et al. Coexpression of CD49b and LAG-3 identifies human and mouse T regulatory type 1 cells. Nat. Med 19, 739–746 (2013). [PubMed: 23624599]
24. Korn T, Bettelli E, Oukka M & Kuchroo VK IL-17 and Th17 cells. Annu. Rev. Immunol 27, 485–517 (2009). [PubMed: 19132915]
25. Maynard CL et al. Regulatory T cells expressing interleukin 10 develop from $Foxp3^+$ and $Foxp3^-$ precursor cells in the absence of interleukin 10. Nat. Immunol 8, 931–941 (2007). [PubMed: 17694059]
26. Sano T et al. An IL-23R/IL-22 circuit regulates epithelial serum amyloid A to promote local effector Th17 responses. Cell 163, 381–393 (2015). [PubMed: 26411290]
27. Wan Q et al. Cytokine signals through PI-3 kinase pathway modulate Th17 cytokine production by CCR6+ human memory T cells. J. Exp. Med 208, 1875–1887 (2011). [PubMed: 21825017]
28. Yadava K et al. Natural Tr1-like cells do not confer long-term tolerogenic memory. eLife 8, e44821 (2019). [PubMed: 31603425]
29. Barrat FJ et al. In vitro generation of interleukin 10-producing regulatory CD4+ T cells is induced by immunosuppressive drugs and inhibited by T helper type 1 (Th1)- and Th2-inducing cytokines. J. Exp. Med 195, 603–616 (2002). [PubMed: 11877483]
30. Song X et al. Microbial bile acid metabolites modulate gut $ROR\gamma^+$ regulatory T cell homeostasis. Nature 577, 410–415 (2020). [PubMed: 31875848]
31. Knott SRV et al. A computational algorithm to predict shRNA potency. Mol. Cell 56, 796–807 (2014). [PubMed: 25435137]
32. Fellmann C et al. An optimized microRNA backbone for effective single-copy RNAi. Cell Rep. 5, 1704–1713 (2013). [PubMed: 24332856]
33. Kim JJ, Shajib MS, Manocha MM & Khan WI Investigating intestinal inflammation in DSS-induced model of IBD. J. Vis. Exp 60, 3678 (2012).
34. Berg DJ et al. Enterocolitis and colon cancer in interleukin-10-deficient mice are associated with aberrant cytokine production and $CD4^+$ TH1-like responses. J. Clin. Invest 98, 1010–1020 (1996). [PubMed: 8770874]
35. Langmead B & Salzberg SL Fast gapped-read alignment with Bowtie 2. Nat. Methods 9, 357–359 (2012). [PubMed: 22388286]
36. Zhang Y et al. Model-based analysis of ChIP-Seq (MACS). Genome Biol 9, R137 (2008). [PubMed: 18798982]
37. Robinson JT et al. Integrative genomics viewer. Nat. Biotechnol. 29, 24–26 (2011). [PubMed: 21221095]
38. Patro R, Duggal G, Love MI, Irizarry RA & Kingsford C Salmon provides fast and bias-aware quantification of transcript expression. Nat. Methods 14, 417–419 (2017). [PubMed: 28263959]
39. Subramanian A et al. Gene set enrichment analysis: a knowledge-based approach for interpreting genome-wide expression profiles. Proc. Natl Acad. Sci. USA 102, 15545–15550 (2005). [PubMed: 16199517]

40. Mootha VK et al. PGC-1α-responsive genes involved in oxidative phosphorylation are coordinately downregulated in human diabetes. Nat. Genet 34, 267–273 (2003). [PubMed: 12808457]

41. Durant L et al. Diverse targets of the transcription factor STAT3 contribute to T cell pathogenicity and homeostasis. Immunity 32, 605–615 (2010). [PubMed: 20493732]

42. Ritchie ME et al. limma powers differential expression analyses for RNA-sequencing and microarray studies. Nucleic Acids Res 43, e47 (2015). [PubMed: 25605792]

43. Wei G et al. Global mapping of H3K4me3 and H3K27me3 reveals specificity and plasticity in lineage fate determination of differentiating CD4+ T cells. Immunity 30, 155–167 (2009). [PubMed: 19144320]

44. Yusuf I et al. Germinal center T follicular helper cell IL-4 production is dependent on signaling lymphocytic activation molecule receptor (CD150). J. Immunol 185, 190–202 (2010). [PubMed: 20525889]

45. Suino K et al. The nuclear xenobiotic receptor CAR: structural determinants of constitutive activation and heterodimerization. Mol. Cell 16, 893–905 (2004). [PubMed: 15610733]

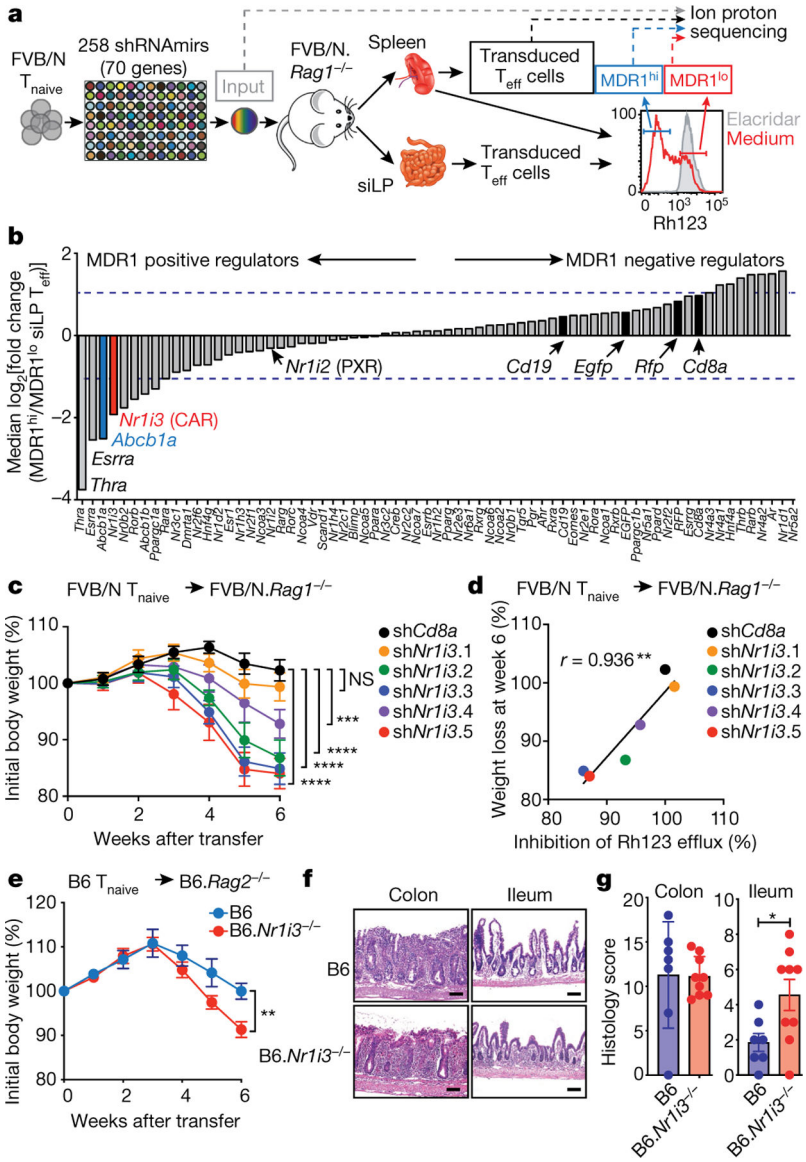

Fig. 1 |. CAR regulates MDR1 expression in CD4$^+$ T cells.

a, Experimental approach for the pooled RNAi screen. T_{naive}, naive T cells. **b**, Median $\log_2$ fold change in shRNAmir abundance between MDR1^{hi} and MDR1^{lo} siLP T_{eff} cells, determined by DNA-seq and grouped by gene (see Supplementary Table 1) in two independent screens. Horizontal dashed lines indicate twofold change. **c**, Mean ± s.e.m. weight loss in co-housed FVB/N.*Rag1*$^{-/-}$ mice that received FVB/N wild-type CD4$^+$ T cells expressing negative control sh*Cd8a* (n = 11) or *Nr1i3*-specific shRNAmirs (sh*Nr1i3*.1 *to* sh*Nr1i3*.5; n = 7 per construct). ***P = 0.0007, ****P < 0.0001, two-way ANOVA; NS, not significant. Data from two independent experiments. **d**, Correlation between T cell transfer-induced weight loss (6 weeks after T cell transfer as in **c**) and MDR1-dependent Rh123 efflux (in week-6 ex vivo-isolated spleen T_{eff} cells as in Extended Data Fig. 1c, d). **P = 0.0059, two-tailed Pearson's correlation test. **e**, Mean ± s.e.m. weight loss in co-housed B6.*Rag2*$^{-/-}$ recipients of wild-type (B6, blue; n = 7) or CAR-deficient (B6.*Nr1i3*$^{-/-}$, red;

$n = 9$) naive $CD4^+$ T cells. $^{**}P = 0.0015$, two-way ANOVA. Data from two independent experiments. **f**, Haematoxylin and eosin (H&E)-stained colon or terminal ileum sections from recipient B6.$Rag2^{-/-}$ mice (6 weeks after T cell transfer as in **e**). Representative of 7–9 mice per group in two independent experiments. Magnification, 10×; scale bars, 100 μm. **g**, Mean ± s.e.m. histology scores for colons or terminal ilea as in **f**. B6.$Rag2^{-/-}$ mice received wild-type (B6; $n = 7$) or CAR-deficient (B6.$Nr1i3^{-/-}$; $n = 9$) T cells. $^{*}P = 0.0447$, unpaired two-tailed Mann–Whitney test.

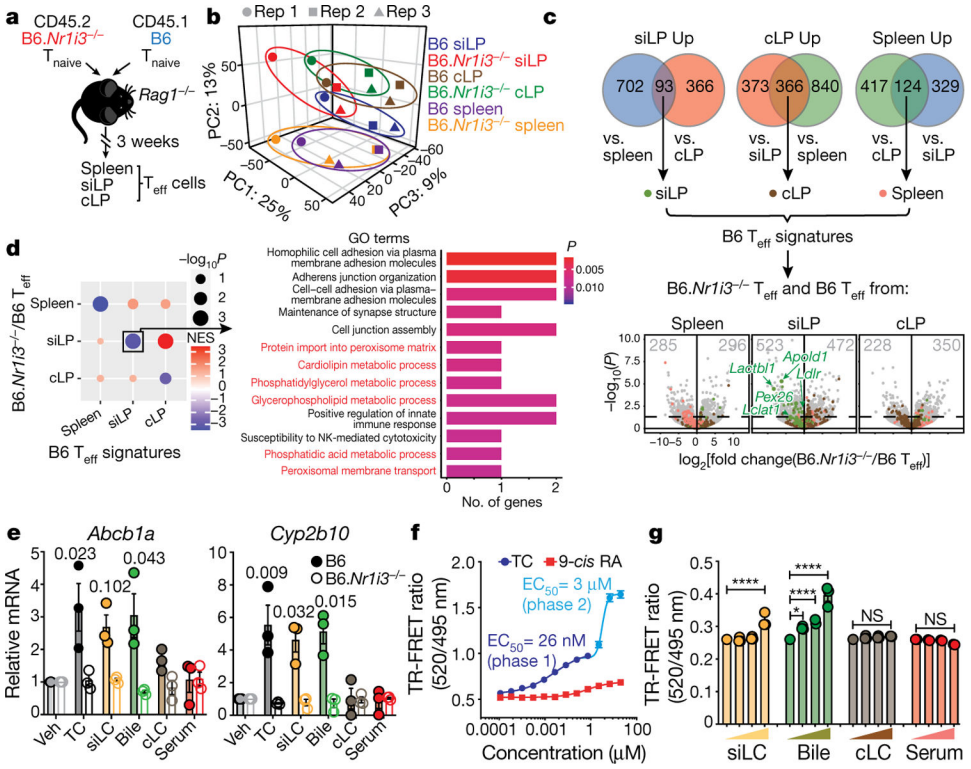

Fig. 2 |. CAR preferentially regulates T cell gene expression in the small intestine.

a, Mixed T cell transfer approach for RNA-seq analysis of wild-type (B6) and CAR-deficient (B6.*Nr1i3*$^{-/-}$) T_{eff} cells. **b**, Principal component analysis (PCA) of gene expression in wild-type and CAR-deficient T_{eff} cells from spleen, siLP and cLP as in **a**. **c**, Top, identification of wild-type T_{eff} cell spleen, siLP or cLP signature genes (Supplementary Table 2). Bottom, differential gene expression between wild-type and CAR-deficient T_{eff} cells by tissue. Up or down gene numbers indicated; exemplar siLP T_{eff}-signature genes highlighted and annotated. **d**, Left, enrichment of wild-type T_{eff} cell tissue-signature genes (*x*-axis, as in **c**) among genes that were differentially expressed between wild-type and CAR-deficient cells by tissue (*y*-axis). NES, normalized enrichment score; nominal *P* values compare observed NESs relative to the null distribution for 1,000 permutations. Right, Gene Ontology (GO) terms that were enriched among CAR-dependent siLP-signature genes; lipid metabolism pathways shown in red. **b–d**, Data from three independent RNA-seq experiments. **e**, Mean ± s.e.m. relative *Abcb1a* and *Cyp2b10* expression ($n = 3$ independent experiments), by qPCR, in ex vivo-isolated wild-type or CAR-deficient T_{eff} cells stimulated with or without mouse tissue extracts. Veh, vehicle. $P < 0.5$ versus vehicle control (one-way ANOVA with Dunnett's correction for multiple comparisons) are shown. **f**, Mean ± s.e.m. ratio of mouse (m)CAR to human (h)RXRα LBD heterodimer activation ($n = 3$ independent experiments) by TR-FRET, with or without TC or 9-*cis* RA (hRXRα agonist). Numbers indicate EC_{50} values. **g**, Mean ± s.e.m. ratio of mCAR:hRXRα LBD heterodimer activation ($n = 3$ independent experiments) by TR-FRET, with or without mouse tissue extracts. Left to right: 0%, 0.01%, 0.1%, 1% extract. $^{*}P = 0.0129$, $^{****}P < 0.0001$, one-way ANOVA with Tukey's correction for multiple comparisons. NS, not significant.

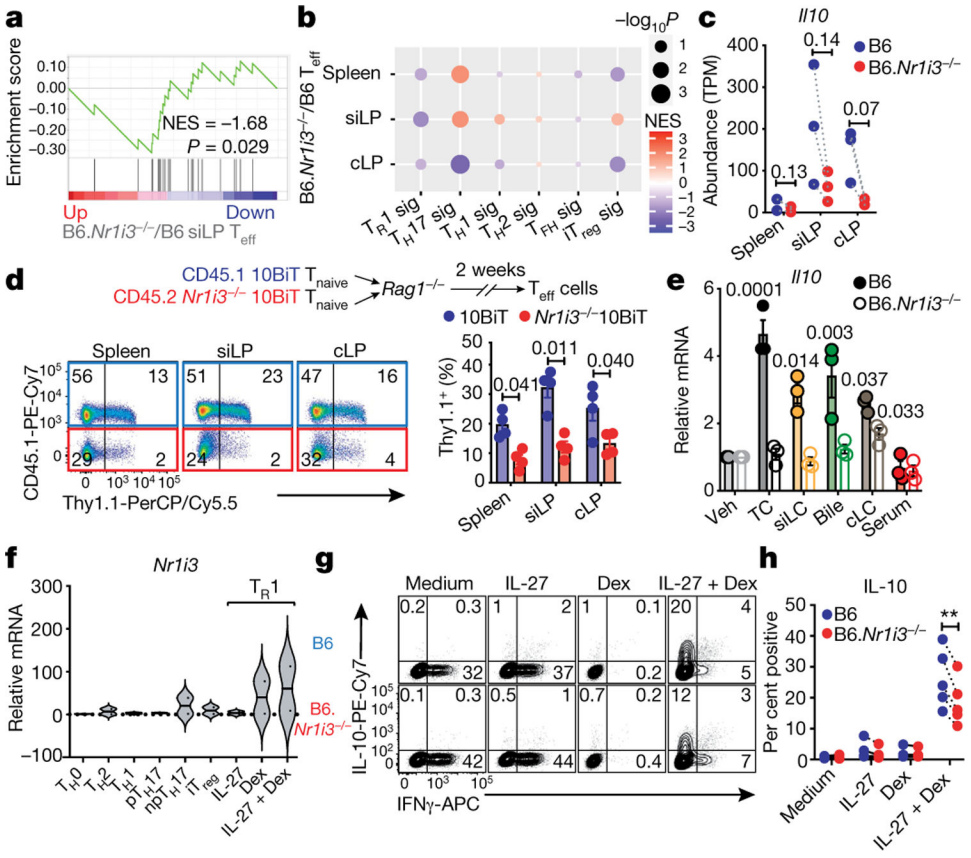

Fig. 3 |. CAR promotes IL-10 expression.

a, Enrichment of T_R1 cell-signature genes[22] among those downregulated in CAR-deficient (B6.*Nr1i3*$^{-/-}$) versus wild-type (B6) siLP T_{eff} cells. **b**, T_H lineage-specific gene set enrichments among genes that were differentially expressed in CAR-deficient versus wild-type T_{eff} cells by tissue. T_{FH}, T follicular helper cell; sig, signature. **a**, **b**, Nominal *P* values compare observed NESs relative to the null distribution for 1,000 permutations. Data from three independent RNA-seq experiments. **c**, *Il10* expression by RNA-seq (n = 3 independent experiments) in wild-type or CAR-deficient T_{eff} cells per tissue. Paired two-tailed Student's *t*-test *P* values shown. **d**, Top, mixed T cell transfer approach for analysing CAR-dependent *Il10*-reporter (Thy1.1)[25] expression. Bottom left, ex vivo Thy1.1-reporter staining in wild-type or CAR-deficient T_{eff} cells by tissue. Representative of four mice in two independent experiments. Bottom right, mean ± s.e.m. Thy1.1$^+$ percentages in wild-type or CAR-deficient T_{eff} cells (n = 4 as above). Paired two-tailed Student's *t*-test *P* values shown. **e**, Mean ± s.e.m. relative *Il10* expression (n = 3 independent experiments) by qPCR in ex vivo-isolated wild-type or CAR-deficient T_{eff} cells stimulated with or without mouse tissue extracts. $P < 0.25$ versus vehicle control (one-way ANOVA with Dunnett's correction for multiple comparisons) are shown. **f**, Mean ± s.e.m. relative *Nr1i3* expression (n = 2 independent experiments) by qPCR in wild-type T cell subsets polarized in vitro. npT$_H$17, non-pathogenic T$_H$17 cells; pT$_H$17, pathogenic T$_H$17 cells. **g**, Intracellular IL-10 and IFN**γ** staining in wild-type or CAR-deficient polarized T_R1 cells. Representative of five

experiments; numbers indicate percentages. **h**, Mean ± s.e.m. IL-10^+ percentages ($n = 5$, as in **g**). ** $P = 0.003$, paired two-tailed Student's t-test.

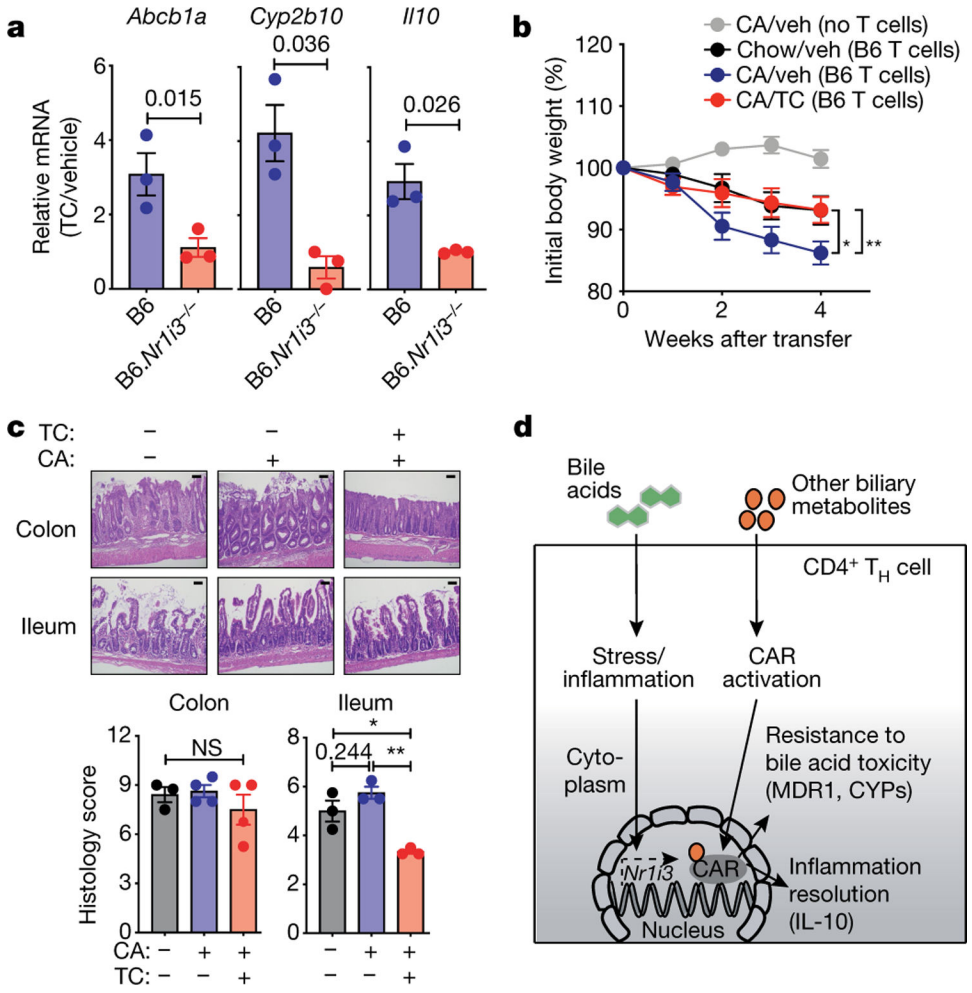

Fig. 4 |. CAR activation in T cells suppresses bile acid-driven ileitis.

a, Mean ± s.e.m. relative *Abcb1a*, *Cyp2b10* or *Il10* expression by qPCR in wild-type (B6) or CAR-deficient (B6.*Nr1i3*$^{-/-}$) spleen T_{eff} cells from co-transferred B6.*Rag1*$^{-/-}$ mice 72 h after treatment with TC or vehicle ($n = 3$ independent experiments). Expression in TC-treated mice relative to vehicle-treated animals. Paired two-tailed Student's *t*-test *P* values shown. **b**, Mean ± s.e.m. weight loss in co-housed *Rag2*$^{-/-}$ mice that received wild-type B6 naive T cells and were fed a cholic acid (CA)-supplemented diet with (red; $n = 18$) or without (blue; $n = 16$) weekly TC treatment. CA-fed *Rag2*$^{-/-}$ mice without T cell transfer (no T cells; grey; $n = 10$); *Rag2*$^{-/-}$ mice that received wild-type T cells left on control chow diet and treated with vehicle (black; $n = 17$). Weights shown relative to initiation of TC treatment (3 weeks after T cell transfer). *$P = 0.031$ (Chow/veh versus CA/veh); **$P = 0.004$ (CA/veh versus CA/TC); two-way ANOVA. Data from three independent experiments. **c**, Top, H&E-stained colon or terminal ileum sections from *Rag2*$^{-/-}$ mice (at 4 weeks after TC treatment as in **b**). Representative of 3–4 mice per group in 2 independent experiments. Magnification, 10× (colons), 20× (ilea); scale bars, 100 μm (colons), 50 μm (ilea). Bottom, mean ± s.e.m. histology scores for colons ($n = 3$–4) or terminal ilea ($n = 3$) as above. *$P = 0.016$, **$P = 0.003$; one-way ANOVA with Tukey's correction for multiple

comparisons. NS, not significant. **d**, Model of CAR-dependent T cell regulation in the small intestine. CYPs, cytochrome P450 enzymes.